Molecular basis of wax-based color change and UV reflection in dragonflies

Ryo Futahashi[1*], Yumi Yamahama[2], Migaku Kawaguchi[3], Naoki Mori[4], Daisuke Ishii[5], Genta Okude[1,6], Yuji Hirai[7], Ryouka Kawahara-Miki[8], Kazutoshi Yoshitake[9], Shunsuke Yajima[8,10], Takahiko Hariyama[2], Takema Fukatsu[1,6,11]

[1]Bioproduction Research Institute, National Institute of Advanced Industrial Science and Technology (AIST), Central 6, Tsukuba, Ibaraki 305-8566, Japan.

[2]Department of Biology, Hamamatsu University School of Medicine, 1-20-1 Handayama, Higashi-ku, Hamamatsu, Shizuoka, 431-3192, Japan.

[3]National Metrology Institute of Japan (NMIJ), National Institute of Advanced Industrial Science and Technology (AIST), Tsukuba Central 3, 1-1-1 Umezono, Tsukuba, Ibaraki 305-8563, Japan.

[4]Division of Applied Life Sciences, Graduate School of Agriculture, Kyoto University, Kyoto 606-8502, Japan

[5]Department of Life Science and Applied Chemistry, Graduate School of Engineering, Nagoya Institute of Technology, Nagoya 466-0059, Japan

[6]Department of Biological Sciences, Graduate School of Science, The University of Tokyo, Tokyo 113-0033, Japan

[7]Applied Chemistry and Bioscience, Chitose Institute of Science and Technology, Chitose 066-8655, Japan

[8]NODAI Genome Research Center, Tokyo University of Agriculture, 1-1-1 Sakuragaoka, Setagaya-ku, Tokyo 156-8502, Japan.

[9]Laboratory of Aquatic Molecular Biology and Biotechnology, Graduate School of Agricultural and Life Sciences, University of Tokyo, Tokyo 113-8657, Japan

[10]Department of Bioscience, Tokyo University of Agriculture, 1-1-1 Sakuragaoka, Setagaya-ku, Tokyo 156-8502, Japan

[11]Graduate School of Life and Environmental Sciences, University of Tsukuba, Tsukuba 305-8577, Japan

[*]For correspondence: ryo-futahashi@aist.go.jp

Tel & Fax: +81-29-861-6812

Abstract

Many animals change their body color for visual signaling and environmental adaptation. Some dragonflies show wax-based color change and ultraviolet (UV) reflection, but biochemical properties underlying the phenomena are totally unknown. Here we investigated the UV-reflective abdominal wax of dragonflies, thereby identifying very long-chain methyl ketones and aldehydes as unique and major wax components. Although little wax was detected on young adults, dense wax secretion was mainly found on the dorsal abdomen in mature males of *Orthetrum albistylum* and *O. melania*, while pruinose wax secretion was identified on the ventral abdomen in mature females of *O. albistylum* and *Sympetrum darwinianum*. Comparative transcriptomics demonstrated drastic upregulation of *ELOVL17* gene, a member of the fatty acid elongase family, whose expression reflected the distribution of very long-chain methyl ketones. Synthetic 2-pentacosanone, the major component of dragonfly's wax, spontaneously formed light-scattering scale-like fine structures with strong UV reflection, suggesting its potential utility for biomimetics.

(150 = 150 words)

Introduction

Many organisms exhibit a variety of body color patterns for visual communication and environmental adaptation. The diversity of the color patterns encompasses the ultraviolet (UV) range, reflecting the fact that many animals can detect UV light as well as green, blue and/or red (Osorio & Vorobyev, 2008). UV reflection has been reported from numerous organisms, which may be important not only for protection against UV-induced damage but also for visual signaling (Silberglied, 1979; Eaton & Lanyon, 2003; Paul & Gwynn-Jones, 2003; Lee, 2007). Previous studies on biological UV reflection have focused on its optical properties and structural bases such as multilayer surface structures (Sun et al., 2013). In some plants and insects, production and secretion of wax on their surface were reported to increase UV reflection (Clark & Lister, 1975; Pope, 1979; Holmes & Keiller, 2002; Kakani et al., 2003).

Dragonflies (including damselflies) are colorful, large-eyed, diurnal and actively-flying insects, whose body colors often markedly differ between sexes, developmental stages, and closely-related species (Tillyard, 1917; Corbet, 1999; Futahashi et al., 2012; Futahashi, 2016; Bybee et al., 2016; Futahashi, 2017). Because dragonflies are able to perceive UV light (Bybee et al., 2012; Futahashi et al., 2015), it seems plausible that UV color also plays important roles in their mate recognition, male-male competition as well as other ecological conditions such as habitat selection and behavioral differences. Several studies have reported that a pruinose wax layer on the body surface accounts for UV reflection patterns in dragonflies (Silberglied, 1979; Robertson, 1984; Hilton, 1986; Gorb, 1995; Harris et al., 2011), but its biochemical properties, molecular composition, and genes involved in the dragonfly's wax production have been totally unknown.

Here, we mainly focus on the white-tailed skimmer dragonfly *Orthetrum albistylum* (Selys, 1848), which is one of the most common dragonfly species in Japan (Sugimura et al., 2001; Ozono et al. 2012). As sexual maturity proceeds, adult males of *O. albistylum* show wax-based body color change from light brown to blueish white, whereas adult females remain brownish throughout most of their lifetime, although very aged females become slightly whitish (Figure 1A) (Sugimura et al., 2001; Ozono et al. 2012). Notably, androchrome females, whose body color is very similar to that of adult males, have been recorded, though very rarely, in the field (Figure 1A) (Sugimura et al., 2001; Ozono et al. 2012). Androchrome females can be distinguished from very aged females because the dorsal abdomen is more whitish than the ventral abdomen after semimature stages (Sugimura et al., 2001; Ozono et al. 2012).

In this study, we investigated the ultrastructure, reflectance, wettability, chemical composition, self-organization, and biosynthesis pathway of surface wax in *O. albistylum* and allied dragonfly species. We found that, during the maturation process, adult males secrete a strongly light-scattering wax layer on the body surface, thereby increasing their visibility not only in the blue and green wavelength ranges but also in the UV range. Chemically, the UV-reflective surface wax consisted of very long-chain methyl ketones and aldehydes, which have not been previously identified as major wax components. Comparative transcriptomics identified a gene belonging to the elongation of very long-chain fatty acids (ELOVL) protein family, whose expression was strongly correlated with the distribution of very long-chain methyl ketones on the surface of dragonflies. Notably, chemically-synthesized 2-pentacosanone, the major component of the surface wax, spontaneously formed scale-like fine structures with strong UV reflection. These results provide a previously undescribed

molecular and structural basis of wax-based body color change and UV reflection with ecological and applied relevance.

Results and Discussion

Stage- and Sex-Dependent Body Color Change and UV Reflection in *O. albistylum*. We compared wax-based body color change and UV reflection patterns of adult insects of *O. albistylum* using a high sensitivity camera with a UV filter. In immature males and females, UV reflection was hardly detected on their body surface (Figure 1B, D, G and I; Video 1). As sexual maturation proceeded, males accumulated whitish wax mainly on the dorsal abdomen, which strongly reflected UV (Figure 1C, F, H and K; Video 1). It should be noted that, in mature females, UV-reflective whitish wax was secreted on the ventral abdomen only (Figure 1D, F, I and K; Video 1). As adult aging proceeded further, not only males but also females developed pruinose wax on the entire body surface (Figure 1A), which resulted in considerable UV reflection even in females. The adult insects of *O. albistylum* were subjected to optical measurements for quantitative evaluation of sex- and stage-dependent changes in reflectance on both the dorsal and ventral abdominal regions. Immature males and females mainly reflected light above 500 nm in wavelength, and did not exhibit remarkable UV reflection (Figure 2A and D-figure supplement 1A and D; Figure 2-source data 1; Figure 2-source data 5). In mature males, reflectance increased, in particular below 600 nm, which resulted in strong UV reflection on the dorsal abdomen and moderate UV reflection on the ventral abdomen (Figure 2B-figure supplement 1B; Figure 2-source data 2; Figure 2-source data 6), whereas in mature females, moderate UV reflection was observed on the ventral abdomen only (Figure 2-figure supplement 1E; Figure 2-source data 2; Figure 2-source data

6). In aged males and females, reflectance increased to some extent on both dorsal and ventral sides of the abdomen (Figure 2C and F-figure supplement 1C and F; Figure 2-source data 3; Figure 2-source data 7). Micro-spectrometry of small areas (10 μm x 10 μm) on the dorsal abdomen of a mature male indicated that the surface wax is responsible for overall reflectance, in particular in the short wavelength range including UV (Figure 2G; Figure 2-source data 4): strong reflection was found in the wax-covered white micro-areas (Figure 2G; a, c, d, e and f) whereas little reflection was detected in the blackish micro-areas where the surface wax was lost (Figure 2G; b, g and h).

Surface Fine Structure of *O. albistylum*. Sex- and stage-dependent changes in the surface fine structure of *O. albistylum*, with special attention to the surface wax, were observed by scanning electron microscopy (SEM). In mature males, the dorsal abdomen was covered with scale- or plate-like fine structures (2–3 μm wide, 50 nm thick), which represented the secreted wax layer (Figure 3A-D and K). The depth of the wax layer reached up to some 6 μm from the cuticle surface (Figure 3D). In mature females and immature individuals, by contrast, only tiny nanopillar-like structures (100 nm wide, 200-300 nm high) were seen on the dorsal abdomen (Figure 3E-J and L). In both mature males and females, on the other hand, small plate-like structures (up to 2 μm wide) were observed on the ventral abdomen, which presumably represented the pruinose wax secretion (Figure 3O and P) that were not conspicuous in immature males and females (Figure 3M and N). Here we suggest that these fractal surface structures consisting of randomly-arranged fine wax platelets are responsible for the whitish structural color due to light scattering, as observed on the dorsal abdomen of mature males and the ventral abdomen of mature males and females. The idea that the

145 secreted wax layer produces structural color was confirmed by a simple experiment: the
146 whitish color disappeared when light scattering was disturbed by acetone application, and the
147 whitish color instantly recovered upon evaporation of the applied acetone (Video 2). Note that
148 the sizes of the wax platelets (up to 2–3 μm) are larger than the wavelength of UV and visible
149 light and thus capable of light scattering, while the sizes of the nanopillar structures (up to
150 200-300 nm) are smaller than the wavelength of UV light and thus incapable of light
151 scattering (Vukusic & Sambles, 2003), and thus the reflectivity at the surface may decrease
152 (Kinoshita & Yoshioka, 2005).
153
154 **Cuticular Fine Structure of *O. albistylum*.** In diverse insects, specialized glands or
155 structures for wax secretion have been characterized (Pope, 1979; Ammar et al., 2015), but
156 such wax-producing structures have not been described from dragonflies. Transmission
157 electron microscopic (TEM) observations of the abdominal ultrathin sections of *O. albistylum*
158 identified a number of fine ducts penetrating the cuticle layer in both immature and mature
159 individuals (Figure 3Q-X). Particularly on the dorsal abdomen of mature males, the cuticular
160 ducts were well-developed and full of electron-dense material, probably reflecting the active
161 wax secretion there (Figure 3S).
162
163 **Chemical Composition of Dragonfly's UV-Reflective Wax.** To investigate the biochemical
164 properties and molecular composition of dragonfly's wax, the surface wax of *O. albistylum*
165 was tested for solubility in organic solvents with reference to surface fine structure and
166 wettability. We found that the secreted wax is insoluble in ethanol (Figure 4B), partially
167 soluble in hexane (Figure 4C and E), and completely soluble in chloroform (Figure 4D and F).

While the untreated abdominal surface exhibited strong water repellency (Figure 4A), removal of the wax by hexane or chloroform treatment resulted in drastically reduced water repellency or increased wettability (Figure 4C and D). As reported in a variety of plants and insects (Hadley, 1981), the strong water repellency conferred by the surface wax may be important for dragonflies with aerial lifestyle to reduce water loss. On the basis of these results, we extracted the surface wax of *O. albistylum* with hexane or chloroform, and analyzed its chemical composition by gas chromatography and mass spectrometry. In the hexane extract from the dorsal abdomen of mature males, only three very long-chain methyl ketones, namely 2-pentacosanone ($C_{25}H_{50}O$), 2-heptacosanone ($C_{27}H_{54}O$) and 2-nonacosanone ($C_{29}H_{58}O$), were identified (Figure 5A-figure supplement 1). In the chloroform extract from the dorsal abdomen of mature males, in addition to the three very long-chain methyl ketones, four very long-chain aldehydes, namely tetracosanal ($C_{24}H_{48}O$), hexacosanal ($C_{26}H_{52}O$), octacosanal ($C_{28}H_{56}O$), and triacosanal ($C_{30}H_{60}O$), were detected (Figure 5B-figure supplement 1). It should be noted that, in mature males, the very long-chain methyl ketones were major on the dorsal abdomen whereas the very long-chain aldehydes were dominant on the ventral abdomen (Figure 5B and C). By contrast, only the four very long-chain aldehydes were identified in the chloroform extract from the ventral abdomen of mature females (Figure 5E), while neither the very long-chain methyl ketones nor the very long-chain aldehydes were found in the chloroform extract from the dorsal abdomen of mature females (Figure 5D). Such very long-chain methyl ketones and aldehydes have been identified, although not existing as major components, from surface wax of plants (Kolattukudy & Walton,1972; Post-Beittenmiller, 1996; Yamamoto et al., 2008; Kunst & Samuels, 2003) and skin lipids of snakes (Ahern et al., 1974). Similar ketones were

characterized as sex pheromones of cockroaches (Nishida et al., 1976) and snakes (Parker & Mason, 2014). In the light of previous studies on wax secretions of various insects, in which hydrocarbons, long-chain esters, alcohols, and/or free fatty acids were identified as major components (Brown, 1975; Blomquist & Jackson, 1979; Hadley, 1981), the chemical composition of the dragonfly's abdominal UV-reflective surface wax seems unique among insects.

Synthetic "Dragonfly Wax" Exhibits Structural Self-Organization, Strong Reflection and Water Repellency. We chemically synthesized 2-pentacosanone, the main UV-reflective wax component identified from the dorsal abdomen of mature males of *O. albistylum* (Figure 5F), and attempted to recrystallize it on glass plates using three methods, namely dropping, quenching, and slow cooling (see Materials and Methods). The dropping method yielded numerous wax platelets randomly arranged on the substratum (Figure 6B and F), which were quite reminiscent of the fine structure of the surface wax on the dorsal abdomen of mature males (Figure 6A and E). By contrast, the quenching method and the slow cooling method resulted in larger wax platelets (Figure 6C, D, G and H), which looked structurally dissimilar to dragonfly's surface wax (Figure 6A and E). The 2-pentacosanone sheets made by the three methods showed qualitatively similar reflectance patterns across UV to visible range, which were also similar to the pattern of dragonfly's surface wax (Figure 6I-L-source data 1). Notably, however, the 2-pentacosanone sheets made by the dropping method yielded stronger light reflectance and lower wettability than those made by the quenching method and the slow cooling method (Figure 6I-P), which are probably due to the smaller wax platelets made by the dropping method that better mimics the fine structure of dragonfly's surface wax.

These results strongly suggest that the light-scattering nanostructure spontaneously formed by the secreted very long-chain methyl ketones, including 2-pentacosanone, should play a pivotal role in formation of the wax layer strongly reflecting UV and visible light on the dorsal abdomen of mature males of *O. albistylum*.

UV-Reflective Wax Production in Other Dragonflies. Diverse dragonfly species are known to secrete whitish or bluish wax on their body surface (Tillyard, 1917; Corbet, 1999; Sugimura et al., 2001; Ozono et al., 2012). In a comparative perspective, we investigated wax production, reflectance, and chloroform-extracted wax composition of the abdominal body surface of three other dragonfly species, *Orthetrum melania*, *Sympetrum darwinianum*, and *Crocothemis servilia* (Figure 7). The blue-tailed skimmer dragonfly *O. melania*, which is closely related to *O. albistylum*, prefers shady habitats in contrast to *O. albistylum* that tends to form territories in sunny places (Sugimura et al., 2001; Ozono et al., 2012). Mature males of *O. melania* develop bluish wax mainly on the dorsal abdomen, whereas mature females do not secrete wax even on the ventral abdomen (Figure 7A). In *O. melania*, UV reflection was observed only on the wax-bearing mature males (Figure 7E, I and L-figure supplement 1A and D; Figure 7-source data 1; Figure 7-source data 4; Video 3). In the red dragonfly *S. darwinianum*, only mature females secrete whitish wax on the ventral abdomen (Figure 7B), where UV reflection was clearly detected (Figure 7F, J and M-figure supplement 1B and E; Figure 7-source data 2; Figure 7-source data 5; Video 3). The scarlet dragonfly *C. servilia* develops little wax on the body surface throughout the lifetime (Figure 7C and D), and UV reflection was not detected in both sexes (Figure 7G, H, K and N-figure supplement 1C and F; Figure 7-source data 3; Figure 7-source data 6). These reflectance data indicated that (i)

presence of the secreted wax on the body surface accounts for the UV-reflecting body regions in all dragonfly species, (ii) meanwhile, the levels of the UV reflection vary among dragonfly species and also across different body regions, and (iii) among them, the dorsal abdomen of mature males of *O. albistylum* exhibits the strongest UV reflection (Figures 2 and 7). The wax composition also varied among dragonfly species (Figure 8). For example, only very long-chain aldehydes were detected from mature males of *O. melania* (Figure 8A and C), while only a very long-chain aldehyde, tetracosanal, was identified from the ventral abdomen of mature females of *S. darwinianum* (Figure 8B and C). Very long-chain methyl ketones were detected only in regions where UV reflection was strong in *O. albistylum* (Figure 8C).

On Ecological Relevance of UV-Reflective Wax Production in Dragonflies. Here we point out that the UV reflection/wax production patterns observed in these dragonflies seem to reflect, at least to some extent, their environmental and behavioral characteristics. In general, body pigmentation and/or wax production are conspicuous in mature dragonflies, especially reproductively-active territorial males (Tillyard, 1917), which may be related to mate recognition, male-male competition, UV protection and anti-desiccation that are fatally important for them (Corbet, 1999). In the closely-related *Orthetrum* species, *O. albistylum* that dominates sunny habitats show stronger UV reflection than *O. melania* that prefers shady habitats: mature males of *O. albistylum* form dense whitish wax layer on the dorsal abdomen (Figure 1C and F; Figure 9A) whereas mature males of *O. melania* develop relatively thin bluish wax layer (Figure 7A; Figure 9B); mature females of *O. albistylum* wear pruinose wax on the ventral abdomen (Figure 1F) while mature females of *O. melania* do not (Figure 7A). Similar patterns are found in other *Orthetrum* species: mature males of *O. luzonicum* prefer

sunny habitats and develop whitish wax (Figure 9C), whereas mature males of *O. glaucum* attach to shady habitats and form bluish wax (Figure 9D). It is intriguing why mature females of some dragonflies produce UV-reflective wax only on the ventral abdomen, as in *O. albistylum* (Figure 1F and K) and *S. darwinianum* (Figure 7B and F). We point out that, in these species, males form territories in sunny places, wait for females that fly in, and chase and copulate with them on nearby plants (Figure 1F; Figure 7B). Therefore, these species usually mate in sunny places, where the female's ventral abdomen is exposed to direct sunshine for an extended period (Figure 1F; Figure 7B). By contrast, *O. melania* usually mates in shady places (Figure 7A), *C. servilia* quickly mates during flight for only a few seconds (Figure 7D), and the female's ventral abdomen develops no wax and exhibits no UV reflection in these species (Figure 7A, D, E and H). Based on these observations, we suggest that, although speculative, the female's ventral wax might be to protect the ventral abdomen, which is less pigmented, less sclerotized and containing ovaries, against UV damage.

Comparative Transcriptomics of Wax-Producing and Non-Producing Epidermal Regions in *O. albistylum*. What molecular mechanisms underlie the production of dragonfly's surface wax of unique chemical composition? Notably, rarely-discovered gynandromorphic dragonflies consistently exhibit discontinuous surface wax patterns (Figure 9E and F) (Sugimura et al., 2001; Karube & Machida, 2015), suggesting that de novo wax production may be regulated in a cell-autonomous manner. In an attempt to gain insights into the molecular basis of dragonfly's wax production, we performed RNA sequencing using samples of the dorsal and ventral abdominal epidermis dissected from immature, semimature, mature, mature-aged, and aged individuals of both sexes of *O. albistylum*. The adult maturity

283 was judged based on the amount of wax and the wing condition. In addition, we were
284 fortunately able to examine a mature androchrome female (Figure 10A). Figure 10B
285 summarizes the RNA sequencing data. Of 7,790 gene models whose max FPKM values were
286 greater than 10, 1,708 genes exhibited twice or higher expression in dorsal epidermis of
287 mature males (with wax) than in that of mature females (no wax); 518 genes exhibited twice
288 or higher expression in dorsal epidermis of an androchrome female (with wax) than that of
289 mature females (no wax); and 305 genes were commonly identified in these two categories as
290 upregulated genes associated with wax production. Of the 305 genes, 26 genes were highly
291 expressed (FPKM > 100), of which 5 genes exhibited extremely high expression levels
292 (FPKM > 1,000) (Figure 10C-figure supplement 1; accession nos. LC416763- LC416767).
293
294 **Drastically Upregulated ELOVL Genes in Wax-Producing Epidermis of *O. albistylum*.**
295 Among the extremely upregulated genes, we identified a gene belonging to the elongation of
296 very long-chain fatty acids (ELOVL) protein family that was drastically and specifically
297 (more than 100-fold) expressed in dorsal epidermis of semimature and mature males and
298 androchrome female (Figure 10C and D-figure supplement 1). ELOVL proteins catalyze the
299 elongation of fatty acids with acyl chains longer than 18 carbon atoms (Kihara, 2012) and also
300 hydrocarbons (Chertemps et al., 2007). ELOVL proteins are conserved from yeast to
301 mammals, and 3, 7 or 20 ELOVL family protein genes are identified in the genome of yeast,
302 mammals or the fruit fly *Drosophila melanogaster*, respectively (Figure 11A)
303 (Szafer-Glusman et al., 2008; Kihara, 2012). In the transcriptomic data of *O. albistylum* and
304 also in the draft genome data of the scarce chaser dragonfly *Ladona fulva* (BCMHGSC: I5K,
305 GenBank accession no. APVN00000000.2), we identified 17 ELOVL genes in total (Figure

306 11A; accession nos. BR001497-BR001513, LC416747-LC416763), all of which contained a
307 conserved HXXHH motif (Figure 11B). In addition to the drastically upregulated ELOVL
308 gene (= *ELOVL17*) mentioned above, two ELOVL genes exhibited notable upregulation
309 patterns (Figure 11C). *ELOVL14* was highly expressed in dorsal epidermis of semimature and
310 mature males, and also in both dorsal and ventral epidermis of androchrome female (Figure
311 10E; Figure 11). In aged females, *ELOVL17* and *ELOVL14* genes were slightly upregulated
312 (Figure 10D and E), which may account for the slight wax secretion on aged females of *O.*
313 *albistylum* (see Figure 1A). Meanwhile, *ELOVL3* gene was preferentially expressed in the
314 ventral abdomen of immature females (Figure 10F), which may be relevant to the preferential
315 accumulation of very long-chain aldehydes on the ventral abdomen of mature females of *O.*
316 *albistylum* (see Figure 5E). These results strongly suggest that these ELOVL genes are
317 involved in production of the surface wax, mainly consisting of very long-chain methyl
318 ketones and aldehydes, of dragonflies. To confirm this idea, we attempted to knock-down the
319 expression level of *ELOVL17* gene by injection of small interfering RNA followed by
320 electroporation, as established in other dragonfly species (Okude et al. 2017). Employing the
321 RNAi treatment, we expected that the wax production on the abdominal surface of mature
322 males would be suppressed. However, because the electroporation damaged the adult cuticle
323 and caused high mortality of the treated insects, we failed to observe the phenotypes expected
324 for the RNAi experiment. Hence, the precise functions of the dragonfly's ELOVL gene
325 products are to be verified in future studies, for which establishment of stable laboratory
326 rearing system for *O. albistylum* and application of genome editing technology to it are
327 anticipated. In addition to *ELOVL17* gene, the following four genes exhibited extremely high
328 expression in wax-producing regions; *Acyl-CoA Delta(11) desaturase*, *ferritin*, *NPC*

329 *intercellular transporter 2*, and *uncharacterized protein* (LC416764- LC416767), although
330 their stage and region specificity was not prominent compared to *ELOVL17* gene. Biological
331 roles of these genes also deserve future studies.
332
333 **Conclusion and Perspective.** In this study, we found that mature males of *O. albistylum*
334 exhibit strong reflection including UV range in a previously uncharacterized way, namely
335 very long-chain methyl ketone production. Plausibly, differences in wax production between
336 sexes, stages and species are important for their signal communications, and may reflect their
337 habitats and behavior. It should be noted that synthesized 2-pentacosanone, a major
338 component of very long-chain methyl ketone, reproduced strong reflection, surface fine
339 structure, and water repellency. Considering that UV reflective materials can be applied in the
340 fields of cosmetics and painting, and *O. albistylum* has been traditionally used as medicine in
341 Asia (Corbet, 1999), the dragonflies' UV reflective wax may be potentially utilized as a novel
342 eco-friendly biological material.
343

344 ## Materials and Methods

345 **Insects and UV images.** Adult insects of *O. albistylum, O. melania*, *S.darwinianum,* and *C.*
346 *servilia* were collected at Tsukuba, Ibaraki, Japan, or Imizu, Toyama, Japan. Photos of UV
347 reflection were taken in the field using a high sensitivity camera (Sony A7S, IDAS UV-VIS
348 mod) through a UV filter (IDAS-U).
349
350 **Spectrometry and micro-spectrometry.** In order to quantitatively investigate the wax-based
351 color change, the dorsal and ventral parts of abdominal segment 5 were surgically divided and

used for reflection measurements. The reflections from small areas (diameter 6 mm) were taken using a spectrometer (HR2000+, Ocean Optics), and those of micro areas (10 x 10 μm) were carried out using a micro-spectrometer (CRAIC Technologies) equipped with an upright microscope (Eclipse E-400; Nikon). The specimens were epi-illuminated with 75 W Xenon arc lamp (Nikon), and the measurements were obtained from an approximately 10 μm x 10 μm area. The reflected spectral radiances were converted to relative reflectance by normalization with a white reflectance standard (Spectralon USRS-99-010, Labsphere).

Histology. The microstructural changes due to wax secretion was examined by scanning electron microscopy (SEM) and transmission electron microscopy (TEM). For SEM observation, the dissected dorsal and ventral parts of the abdominal segment 5 were coated with 2-3 nm osmium layer using a hollow-cathode plasma chemical vapor deposition (HPC-1SW; Vacuum Device), and observed under a scanning electron microscope (H-4800; Hitachi) with an accelerating voltage of 5 kV. For TEM observation, dissected dorsal and ventral parts of the abdominal segment 5 were prefixed for 12 h in 2% glutaraldehyde and 2% paraformaldehyde in 0.1 M cacodylate buffer (pH7.2), post-fixed with 1% osmium tetroxide for 2 h in 0.1 M cacodylate buffer, and embedded in Quetol 812-Araldite regin mixture (Nisshin EM). Ultrathin sections (approximately 70nm thick) were cut perpendicular to the anterior-posterior axis on an ultra-microtome (UC7; Leica) with a diamond knife (DiATOME), stained with 2% uranyl acetate for 5 min followed by lead citrate solution for 3 min (Sigma-Aldrich), and observed under a transmission electron microscope (JEM-1400; JEOL, 100 KV).

Measurement of surface wettability and wax solubility. To elucidate the biochemical properties of dragonfly's wax, surface wettability and solubility was examined. Surface wettability was evaluated based on the contact angle of water micro-droplet on the samples. Each sample was fixed on a glass substrate, and a micro-droplet of distilled water (about 1.0 nL) was placed on the surface of the sample. The shape of droplet was recorded immediately using a high-speed camera (HAS-220; Ditect) with a microscopic contact angle meter (MCA-3; Kyowa Interface Science). Wax solubility was analyzed by treating the dissected abdominal segment 5 with hexane or chloroform for 30 min.

Wax extraction and analysis. To identify the molecular composition of dragonfly's wax, wax samples were extracted from living specimens with chloroform or hexane. For gas chromatography/mass spectrometry (GC-MS) analysis, to avoid contamination from internal lipids, the solvent was carefully pipetted several times on the abdominal surface of the living individuals. The extracts were analyzed by GC-MS using a 6890N GC coupled with 5973 MSD (Agilent) in the split-less mode, through a DB-5MS fused silica column (30 m x 0.25 mm i.d., 0.25 μm film thickness, Agilent) with helium as the carrier gas at a flow rate of 1.0 mL/min at a temperature programmed to change from 80°C (1 min) to 320°C at a rate of 15°C/min and then held for 3 min. The mass spectrometer was operated in the scan mode with 70 eV ionazation voltage as electron ionization. Histological examinations, wettability tests, and GC-MS analyses were conducted using different samples.

Chemical synthesis of wax components. To confirm whether the very long-chain methyl ketones form the scale-like fine structures, 2-pentacosanone, the major component of

dragonfly's wax was chemically synthesized from 1-tetracosanol via 1-tetracosanal and 2-pentacosanol. Pyridinium chlorochromate (PCC, 1.29 g, 5.97 mmol) was added to a suspension of 1-tetracosanol (395 mg, 1.11 mmol) and powdered molecular sieves 4A (2.5 g) in dry CH_2Cl_2 (35 mL), and stirred for 4 h at room temperature. The mixture was filtered through Celite and washed with diethyl ether. The combined filtrate and washings were filtered through florisil (15 g), washed with diethyl ether (200 mL) and concentrated *in vacuo*. The residue was chromatographed on silica gel (15 g) and concentrated *in vacuo* to give a white solid of 1-tetracosanal (290 mg, 0.82 mmol, 74%, GC t_R = 23.7 min, MS *m/z* (%): 352 (M^+, 2), 334 (18), 96 (78), 82 (100), 57 (93), 43(72).). A solution of 1-tetracosanal (176 mg, 0.50 mmol) in dry tetrahydrofuran (THF, 10 mL) was cooled in ice bath. When the temperature reached 0°C, 1.4 M CH_3MgBr in THF:toluene 1:3 (1 mL, 1.4 mmol) was added dropwise, and stirred for 1.5 h at 0°C and for 1 h at room temperature. The reaction was quenched with saturated NH_4Cl (5 mL), and the product was extracted with hexane (3 × 20 mL). The organic layer was dried with anhydrous magnesium sulfate and concentrated *in vacuo*. The residue was chromatographed on silica gel (15 g, ethyl acetate/hexane, 1:5) to give a white solid of 2-pentacosanol (106 mg, 0.29 mmol, 58%). PCC (335 mg, 1.56 mmol) was added to a suspension of 2-pentacosanol (257 mg, 0.70 mmol) and powdered molecular sieves 4A (1.0 g) in dry CH_2Cl_2 (20 mL), and stirred for 3 h at room temperature. The mixture was filtered through Celite and washed with diethyl ether. The combined filtrate and washings were filtered through florisil (15 g), washed with diethyl ether (200 mL) and concentrated *in vacuo*. The residue was recrystallized from hexane to give a white solid of 2-pentacosanone (202 mg, 0.55 mmol, 76%). Nuclear magnetic resonance (NMR) spectra of 2-pentacosanal and 2-pentacosanone were measured with Bruker AV-400 III

421 Spectrometer (400 MHz) using TMS as an internal standard. Each sample was dissolved in
422 $CDCl_3$ and ^1H spectrum was acquired. ^1H-NMR of 2-pentacosanal ($CDCl_3$, 400 MHz) was as
423 follows: δ 3.79 (1H, sex, *J*=6.0 Hz, H-2), δ 1.18 (3H, d, *J*=6.0 Hz, H-1), δ 0.88 (3H, t,
424 *J*=6.0 Hz, H-25). ^1H-NMR of 2-pentacosanone ($CDCl_3$, 400 MHz) is as follows: δ 2.41 (2H,
425 d, *J*=7.6 Hz, H-3), δ 2.13 (3H, s, H-1), δ 0.88 (3H, t, *J*=6.4 Hz, H-25).
426
427 **Preparation of biomimetic wax surfaces.** Biomimetic wax surfaces were composed of
428 micro crystals of 2-pentacosanone. Heated 2-pentacosanone was recrystallize on gold-coated
429 glass plates by different cooling processes; 1) continuous dropping of micro fused material of
430 1.0 μL under room temperature, 2) quenching from the melting state, and 3) keeping to near
431 melting point at 64°C from the melting state. Micro-spectrometry, surface fine structure, and
432 wettability were analyzed using a micro-spectrometer (CRAIC Technologies), a scanning
433 electron microscope (H-4800; Hitachi), or a high-speed camera (HAS-220; Ditect) with a
434 microscopic contact angle meter (MCA-3; Kyowa Interface Science), respectively, as
435 described above.
436
437 **Transcriptome Analysis.** To investigate the genes involved in wax production, total RNA
438 samples were extracted from the freshly dissected abdomens of *O. albistylum* using RNeasy
439 mini kit (Qiagen) or Maxwell 16 LEV Simply RNA Tissue kit (Promega). RNA sequencing
440 was performed as described previously (Futahashi et al., 2015). Using 1 μg of total RNA per
441 sample as template, cDNA libraries were constructed using TruSeq RNA Sample Preparation
442 Kits v2 (Illumina) and sequenced by HiSeq2000, Hiseq2500, or MiSeq (Illumina). The
443 sequence data were deposited in the DNA Data Bank Japan Sequence Read Archive

(accession numbers are shown in Supplementary File 1). The raw reads were subjected to de novo assembling using the Trinity program (Grabherr et al., 2011) implemented in the MASER pipeline (Kinjo et al., 2018). After automatic assembling, we checked and manually corrected the sequences of highly expressed genes in mature males using the Integrative Genomics Viewer (Thorvaldsdóttir et al., 2013) as reported previously (Futahashi, 2017). After revising the sequences, sequence read mapping was performed using the BWA-MEM program (Li, 2013) implemented in the MASER pipeline, whereby transcript expression levels were estimated in terms of fragments per kilobase per million reads (FPKM) values. ELOVL genes of *L. fulva* were obtained by tBLASTn search against the draft genome sequence (APVN00000000.2) (https://www.hgsc.bcm.edu/).

Phylogenetic analysis. To construct the molecular phylogeny of ELOVL family genes, deduced amino acid sequences were aligned using the Clustal W program implemented in MEGA7 (Kumar et al., 2016). Molecular phylogenetic analyses were conducted by the neighbor-joining method and maximum-likelihood method using MEGA7, and by the Bayesian method using MrBayes version 3.1.2 (Ronquist et al., 2012). Bootstrap values for neighbor-joining and maximum likelihood phylogenies were obtained by 1000 resampling. In total 3750 trees were generated for each Bayesian analysis (ngen = 500,000, samplefreq = 100, burn in = 1250).

ACKNOWLEDGMENTS. We thank Tateo Shimozawa for SEM observation, Hiroyuki Futahashi for insect samples, Mitsutoshi Sugimura and Makoto Machida for photos of gynandromorphic dragonflies in Figure 9, and Mutsuo Tanaka and Minoru Moriyama for

technical assistance. We would like to acknowledge i5K, Stephen Richards and Oliver Niehuis for allowing us to use the *L. fulva* genome data. This work was supported by the Japan Society for the Promotion of Science Grant-in-Aid for Scientific Research Grants JP26660276, JP18H02491, and JP18H04893 (to R.F.), and the Cooperative Research Grant of the Genome Research for BioResource, NODAI Genome Research Center, Tokyo University of Agriculture (to R.F., R.M.K., and S.Y). This research was partially supported by Platform Project for Supporting Drug Discovery and Life Science Research (Basis for Supporting Innovative Drug Discovery and Life Science Research (BINDS)) from AMED under Grant Number JP17am0101001.

Data deposition: The sequences reported in this paper have been deposited in the DNA Data Bank Japan Read Archive, www.ddbj.nig.ac.jp (accession nos. BR001497-BR001513, LC416747-LC416767, DRA001687, DRA001690, DRA001693-DRA001694, DRA001697-DRA001698, DRA001700-DRA001701, DRA001703-DRA001704, DRA001706-DRA001707, DRA001709-DRA001710, DRA001712-DRA001713, DRA001716-DRA001717, DRA007015-DRA007018).

Competing interests:

We filed an international patent on the synthesis method and application of very long-chain methyl ketones and aldehydes as PCT/JP2018/019559.

References

Ahern DG, Downing DT (1974) Skin lipids of the Florida indigo snake. *Lipids* 9: 8-14.

490 Ammar el-D, Hentz M, Hall DG, Shatters RG Jr. (2015) Ultrastructure of Wax-Producing
491 Structures on the Integument of the Melaleuca Psyllid Boreioglycaspis melaleucae
492 (Hemiptera: Psyllidae), with Honeydew Excretion Behavior in Males and Females. *PLoS*
493 *One* 10(3): e0121354.
494 Blomquist GJ, Jackson LL (1979) Chemistry and biochemistry of insect waxes. *Prog Lipid*
495 *Res* 17: 319-345.
496 Brown KS (1975) The Chemistry of Aphids and Scale Insects. *Chem Soc Rev* 4: 263-288.
497 Bybee S, Cordoba-Aguilar A, Duryea MC, Futahashi R, Hansson B, Lorenzo-Carballa MO,
498 Schilder R, Stoks R, Suvorov A, Svensson EI, Swaegers J, Takahashi Y, Watts PC,
499 Wellenreuther M (2016) Odonata (dragonflies and damselflies) as a bridge between ecology
500 and evolutionary genomics. *Front Zool* 13: 46.
501 Bybee SM, Johnson KK, Gering EJ, Whiting MF, Crandall KA (2012) All the better to see
502 you with: a review of odonate color vision with transcriptomic insight into the odonate eye.
503 *Org Divers Evol*, 12: 241-250.
504 Chertemps T, Duportets L, Labeur C, Ueda R, Takahashi K, Saigo K, Wicker-Thomas C
505 (2007) A female-biased expressed elongase involved in long-chain hydrocarbon
506 biosynthesis and courtship behavior in *Drosophila melanogaster*. *Proc Natl Acad Sci U S A*.
507 104(11): 4273-4278.
508 Clark JB, Lister GR (1975) Photosynthetic action spectra of trees II. The relationship of
509 cuticle structure to the visible and ultraviolet spectral properties of needles from four
510 coniferous species. *Plant Physiol* 55: 407-413.
511 Corbet, PS (1999) *Dragonflies, Behavior and Ecology of Odonata*. Cornell University Press.
512 Eaton MD, Lanyon SM (2003) The ubiquity of avian ultraviolet plumage reflectance. *Proc. R.*

513 *Soc. Lond. B*, 270: 1721–1726.
514 Futahashi (2016) Color vision and color formation in dragonflies. *Curr Opin Insect Sci*, 17:
515 32-39.
516 Futahashi R. (2017) Molecular Mechanisms Underlying Color Vision and Color Formation in
517 Dragonflies. *Diversity and Evolution of Butterfly Wing Patterns: An Integrative Approach*,
518 eds. Sekimura T, Nijhout HF (Springer, Singapore), pp 303-321.
519 Futahashi R, Kurita R, Mano H, Fukatsu T (2012) Redox alters yellow dragonflies into red.
520 *Proc Natl Acad Sci USA*, 109(31): 12626-12631.
521 Futahashi R., Kawahara-Miki R., Kinoshita M., Yoshitake K., Yajima S., Arikawa K., Fukatsu
522 T (2015) Extraordinary diversity of visual opsin genes in dragonflies. *Proc Natl Acad Sci*
523 *USA*, 112(11): E1247-E1256.
524 Gorb SN (1995) Scanning electron microscopy of pruinosity in Odonata. *Odonatologica*,
525 24(2): 225-228.
526 Grabherr MG, Haas BJ, Yassour M, Levin JZ, Thompson DA, Amit I, Adiconis X, Fan L,
527 Raychowdhury R, Zeng Q, Chen Z, Mauceli E, Hacohen N, Gnirke A, Rhind N, di Palma F,
528 Birren BW, Nusbaum C, Lindblad-Toh K, Friedman N, Regev A (2011) Full-length
529 transcriptome assembly from RNA-Seq data without a reference genome. *Nat Biotechnol*.
530 29(7): 644-652.
531 Hadley NF (1981) Cuticular lipids of terrestrial plants and arthropods: a comparison of their
532 structure, composition, and waterproofing function. *Biol Rev* 56(1): 23-47.
533 Harris WE, Forman DW, Battell RD, Battell MTR, Nelson AK, Brain PF (2011) Odonata
534 colour: more than meets the eye? *Int J Odonatol* 14(3): 281-289.
535 Hilton DFJ (1986) A survey of some Odonata for ultraviolet patterns. *Odonatologica*, 15(3):

335-345.

Holmes MG, Keiller D (2002) Effects of pubescence and waxes on the reflectance of leaves in the ultraviolet and photosynthetic wavebands: a comparison of a range of species. *Plant Cell Environ* 25: 85-93.

Kakani VG, Reddy KR, Zhao D, Sailaja K (2003) Field crop responses to ultraviolet-B radiation: a review. *Agric For Meteorol* 120: 191-218.

Karube H, Machida M (2015) Record of a gynandromorphic individual of *Lyriothemis pachygastra* (Selys, 1878) (Anisoptera: Libellulidae). *Tombo* 57: 43-45.

Kihara A (2012) Very long-chain fatty acids: elongation, physiology and related disorders. *J Biochem* 152: 387-395.

Kinjo S, Monma N, Misu S, Kitamura N, Imoto J, Yoshitake K, Gojobori T, Ikeo K (2018) Maser: one-stop platform for NGS big data from analysis to visualization. *Database (Oxford)*. 2018 Jan 1;2018. doi: 10.1093/database/bay027.

Kinoshita S, Yoshioka S (2005) Structural colors in nature: the role of regularity and irregularity in the structure. *Chemphyschem*. 6(8): 1442-1459.

Kolattukudy PE, Walton TJ (1972) The biochemistry of plant cuticular lipids. *Prog Chem Fats Other Lipids* 13(3): 119-175.

Kumar S, Stecher G, Tamura K (2016) MEGA7: Molecular Evolutionary Genetics Analysis Version 7.0 for Bigger Datasets. *Mol Biol Evol* 33(7): 1870–1874.

Kunst L, Samuels AL (2003) Biosynthesis and secretion of plant cuticular wax. *Progr Lipid Res* 42: 51-80.

Lee D (2007) *Nature's Palette: The Science of Plant Color*. University Chicago Press, Chicago.

559 Li H (2013) Aligning sequence reads, clone sequences and assembly contigs with
560 BWA-MEM. arXiv:1303.3997 [q-bio.GN].
561 Nishida R, Sato T, Kuwahara Y, Fukami H, Ishii SJ (1976) Female sex pheromone of the
562 german cockroach, *Blattella germanica* (L.) (Orthoptera: Blattellidae), responsible for male
563 wing-raising II. 29-Hydroxy-3,11-dimethyl-2-nonacosanone. *J Chem Ecol* 2: 449-455.
564 Okude G, Futahashi R, Kawahara-Miki R, Yoshitake K, Yajima S, Fukatsu T (2017)
565 Electroporation-mediated RNA interference reveals a role of multicopper oxidase 2 gene in
566 dragonfly's cuticular pigmentation. *Appl Entomol Zool* 53(3): 379-387.
567 Osorio D, Vorobyev M (2008) A review of the evolution of animal colour vision and visual
568 communication signals. *Vision Res* 48(20): 2042-2051.
569 Ozono A, Kawashima I, Futahashi R (2012) *Dragonflies of Japan*, Bunichi-Sogo Syuppan.,
570 Co. Ltd.
571 Parker MR, Mason RT (2014) A novel mechanism regulating a sexual signal: The
572 testosterone-based inhibition of female sex pheromone expression in garter snakes. *Horm*
573 *Behav* 66(3): 509-516.
574 Paul ND, Gwynn-Jones D (2003) Ecological roles of solar UV radiation: towards an
575 integrated approach. *Trends Ecol Evol* 18: 48-55.
576 Pope RD (1979) Wax production by coccinellid larvae (Coleoptera), Systematic Entomology,
577 4: 171-196.
578 Post-Beittenmiller D (1996) Biochemistry and molecular biology of wax production in plants.
579 *Annu Rev Plant Physiol Plant Mol Biol* 47: 405-430.
580 Robertson HM (1984) Pruinosity in odonates reflects UV. *Nolul Odonatol* 2: 68-69.
581 Ronquist F, Teslenko M, van der Mark P, Ayres DL, Darling A, Höhna S, Larget B, Liu L,

582 Suchard MA, Huelsenbeck JP (2012) MrBayes 3.2: efficient Bayesian phylogenetic
583 inference and model choice across a large model space. *Syst Biol* 61: 539–542.
584 Silberglied RE (1979) Communication in the Ultraviolet. *Ann Rev Ecol Syst*, 10: 373-398.
585 Sugimura M, Ishida S, Kojima K, Ishida K, Aoki T (2001) *Dragonflies of the Japanese*
586 *Archipelago in color*. Hokkaido University Press.
587 Sun J, Bhushan B, Tong J (2013) Structural coloration in nature. *RSC Adv* 3: 14862-14889.
588 Szafer-Glusman E, Giansanti MG, Nishihama R, Bolival B, Pringle J, Gatti M, Fuller MT
589 (2008) A role for very-long-chain fatty acids in furrow ingression during cytokinesis in
590 *Drosophila* spermatocytes. *Curr Biol* 18: 1426-1431.
591 Thorvaldsdóttir H, Robinson JT, Mesirov JP (2013) Integrative Genomics Viewer (IGV):
592 high-performance genomics data visualization and exploration. Brief Bioinform. 14:
593 178-192.
594 Tillyard, B.J. (1917) *The Biology of Dragonflies*. Cambridge University Press.
595 Vukusic P, Sambles JR (2003) Photonic structures in biology. *Nature* 424(6950): 852-855.
596 Yamamoto S, Otto A, Simoneit BRT (2008) GC-MS analysis of wax in leaf of
597 *Sequoiadendron giganteum*, Sequoioideae, Cuprressaceae. *Res Org Geochem* 23/24,
598 159-171.
599

600 ## Figure Captions

601 **Figure 1.** Stage- and sex-dependent adult color change in *O. albistylum*. (A) Adult males and
602 females of *O. albistylum*. (B, G) Immature male. (C, H) Mature male. (D, I) Immature female.
603 (E, J) Mature female. (F, K) Mating pair. Images photographed normally (B-F) or through a
604 UV filter (G-K) in the field.

Figure 2. Reflectance on the adult body surface at the 5th abdominal segment of *O. albistylum*. (A-F) Spectrometry of a round area (6 mm in diameter) in males (A-C) and females (D-F). (A, D) Immature individuals. (B, E) Mature individuals. (C, F) Aged individuals. Solid and dotted lines indicate averaged UV reflectance on dorsal and ventral sides of the abdomen, respectively. The standard deviation is shaded. (G) Micro-spectrometry of the 5th abdominal segment of a mature male. UV reflectance was measured of eight micro-areas (10 μm x 10 μm each) depicted as red squares in the photos. In the photos, white areas are covered with secreted wax whereas black areas are without wax presumably due to accidental scratches and cracks of the adult body surface.

Figure supplement 1. Micro-spectrometry (10 x 10 μm) of *O. albistylum*. (A-C) Male. (D-F) Female. (A, D) Immature individuals. (B, E) Mature individuals. (C, F) Aged individuals. Three to eight micro-areas were measured for each individual.

Figure 3. Fine structure of the adult body surface at the 5th abdominal segment of *O. albistylum*. (A-P) Scanning electron microscopic (SEM) images of the body surface. (Q-X) Transmission electron microscopic (TEM) images of the sectioned cuticle. Here it should be noted that surface wax was dissolved and removed during the sample processing for TEM observation. (A-H) Dorsal side of mature male (A-D) and mature female (E-H). Panels B and F are magnified images of panels A and E, as indicated by red rectangles. Likewise, panels C and G are magnified images of panels B and F. (D, H) Cross-sectioned images of cuticle and surface wax. (I-L and Q-T) Dorsal side. (M-P and U-X) Ventral side. (I, M, Q, U) Immature male. (J, N, R, V) Immature female. (K, O, S, W) Mature male. (L, P, T, X) Mature female.

628

629 **Figure 4.** Solubility and wettability of the abdominal wax of *O. albistylum*. (A-D) Dorsal side
630 of the 5th abdominal segment of mature males. (A) No treatment. (B) After ethanol treatment.
631 (C) After hexane treatment. (D) After chloroform treatment. (E) Scanning electron
632 microscopic images of dorsal surface of mature male 30 min after hexane treatment. (F)
633 Scanning electron microscopic images of dorsal side of mature male (left) or mature female
634 (right) after chloroform treatment.

635

636 **Figure 5.** Identification and chemical synthesis of surface wax of *O. albistylum.* (A)
637 Chromatogram of hexane extract from the dorsal abdomen of mature male. (B)
638 Chromatogram of chloroform extract from the dorsal abdomen of mature male. (C)
639 Chromatogram of chloroform extract from the ventral abdomen of mature male. (D)
640 Chromatogram of chloroform extract from the dorsal abdomen of mature female. (E)
641 Chromatogram of chloroform extract from the ventral abdomen of mature female. (F)
642 Chromatogram of chemically-synthesized 2-pentacosanone. Asterisks indicate nonspecific
643 peaks also detected with the solvent only. The Y-axis shows the abundance of total ion
644 current.

645 **Figure supplement 1.** Mass spectra and extracted ion chromatogram of dragonfly's wax (A,
646 B, D-H) and synthetic 2-pentacosanone (C).

647

648 **Figure 6.** Comparison of surface fine structure, reflectance, and wettability among the dorsal
649 abdomen of mature males of *O. albistylum* and synthetic 2- pentacosanone crystallized on
650 glass plates using three different cooling processes. (A-H) Scanning electron microscopic

651 images. Panels E, F, G and H are magnified images of panels A, B, C and D, respectively, as
652 indicated by red rectangles. (I-L) Micro-spectrometry on 10 μm x 10 μm area. (M-P)
653 Wettability measured with 1 nL water droplet. (A, E, I, M) The dorsal abdomen of mature
654 males of *O. albistylum*. (B, F, J, N) Synthetic wax crystallized by dropping method. (C, G, K,
655 O) Synthetic wax crystallized by quenching method. (D, H, L, P) Synthetic wax crystallized
656 by slow cooling method.
657
658 **Figure 7.** UV reflection patterns in *O. melania*, *S. darwinianum* and *C. servilia*. (A, E)
659 Mating pair of *O. melania* (B, F) Mating pair of *S. darwinianum.* (C, G) Mature male of *C.*
660 *servilia* with mature male of *O. albistylum*. (D, H) Mating pair of *C. servilia*. Each image
661 photographed normally (A-D) or through a UV filter (E-H) in the field. (I-N) Spectrometry of
662 a round area (6 mm in diameter) on the 5^{th} abdominal segment of *O. melania* (I, L), *S.*
663 *darwinianum* (J, M), and *C. servilia* (K, N). (I-K) Male. (L-N) Female. Solid and dotted lines
664 indicate averaged UV reflectance on dorsal and ventral sides of the abdomen, respectively.
665 The standard deviation is shaded.
666 **Figure supplement 1.** Micro-spectrometry (10 x 10 μm) of *O. melania* (A, D), *S.*
667 *darwinianum* (B, E), and *C. servilia* (C, F). (A-C) Male. (D-F) Female. Five to ten
668 micro-areas were measured for each individual.
669
670 **Figure 8.** Comparison of wax components on the dorsal and ventral abdomen of *O.*
671 *albistylum, O. melania* and *S. darwinianum.* (A) Chromatogram of chloroform extract from
672 the dorsal abdomen of mature male of *O. melania*. (B) Chromatogram of chloroform extract
673 from the ventral abdomen of mature female of *S. darwinianum*. Asterisks indicate nonspecific

674 peaks also detected with the solvent only. (C) Summary of wax components detected from *O.*
675 *albistylum, O. melania* and *S. darwinianum.* Relative amount was judged from the abundance
676 of total ion current. +++, high amount; ++, moderate amount; +, small amount.
677
678 **Figure 9.** Surface wax of *Orthetrum* species and allied dragonflies. (A-D) Mature males of *O.*
679 *albistylum* (A), *O. melania* (B), *O. luzonicum* (C) and *O. glaucum* (D). (E-F)
680 Gynandromorphic individuals of *O. japonimum* (E) and *Lyriothemis pachygastra* (F). Photos
681 courtesy of Mitsutoshi Sugimura (E) and Makoto Machida (F).
682
683 **Figure 10.** Genes associated with UV reflective wax. (A) An androchrome female used for
684 transcriptome analysis. (B) The number of genes upregulated in the dorsal abdominal
685 epidermis of males and/or an androchrome female compared to normal females. (C) The list
686 of genes upregulated in the dorsal abdominal epidermis of both males and an androchrome
687 female (max FPKM > 1000). Gene expression levels are displayed by heat map. The numbers
688 indicate FPKM values. Red and blue indicate high and low expression levels, respectively. D
689 and V indicate the dorsal and ventral abdominal region, respectively. (D-F) Expression level
690 of three Elongation of very long-chain fatty acids (ELOVL) genes in dorsal and ventral parts
691 of epidermis of *O. albistylum.*
692 **Figure supplement 1.** The list of genes upregulated in the dorsal abdominal epidermis of
693 both males and an androchrome female (max FPKM > 100). Gene expression levels are
694 displayed by heat map. The numbers indicate FPKM values. Red and blue indicate high and
695 low expression levels, respectively. D and V indicate the dorsal and ventral abdominal region,
696 respectively. Andro and Gyno mean androchrome and normal (gynochrome) females,

respectively.

Figure 11. Identification of 17 ELOVL genes in dragonflies. (A) Phylogenetic tree of ELOVL family genes on the basis of their amino acid sequences. A maximum likelihood phylogeny is shown, while neighbor-joining and Bayesian phylogenies exhibit substantially the same topologies. Statistical supporting values are indicated on each node in the order of (bootstrap value of neighbor-joining)/(bootstrap value of maximum likelihood)/(posterior probability of Bayesian). Asterisks indicate support values < 50%. Blue and gray shade indicate *O. albistylum* and *L. fulva* genes, respectively. Accession numbers or annotation identities are shown in parentheses. (B) Alignment of 17 ELOVL genes of *O. albistylum*. The conserved histidine motif is boxed. (C) Gene expression levels of 17 ELOVL genes in *O. albistylum*. The numbers indicate FPKM values. Red and blue indicate high and low expression levels, respectively. D and V indicate the dorsal and ventral abdominal region, respectively.

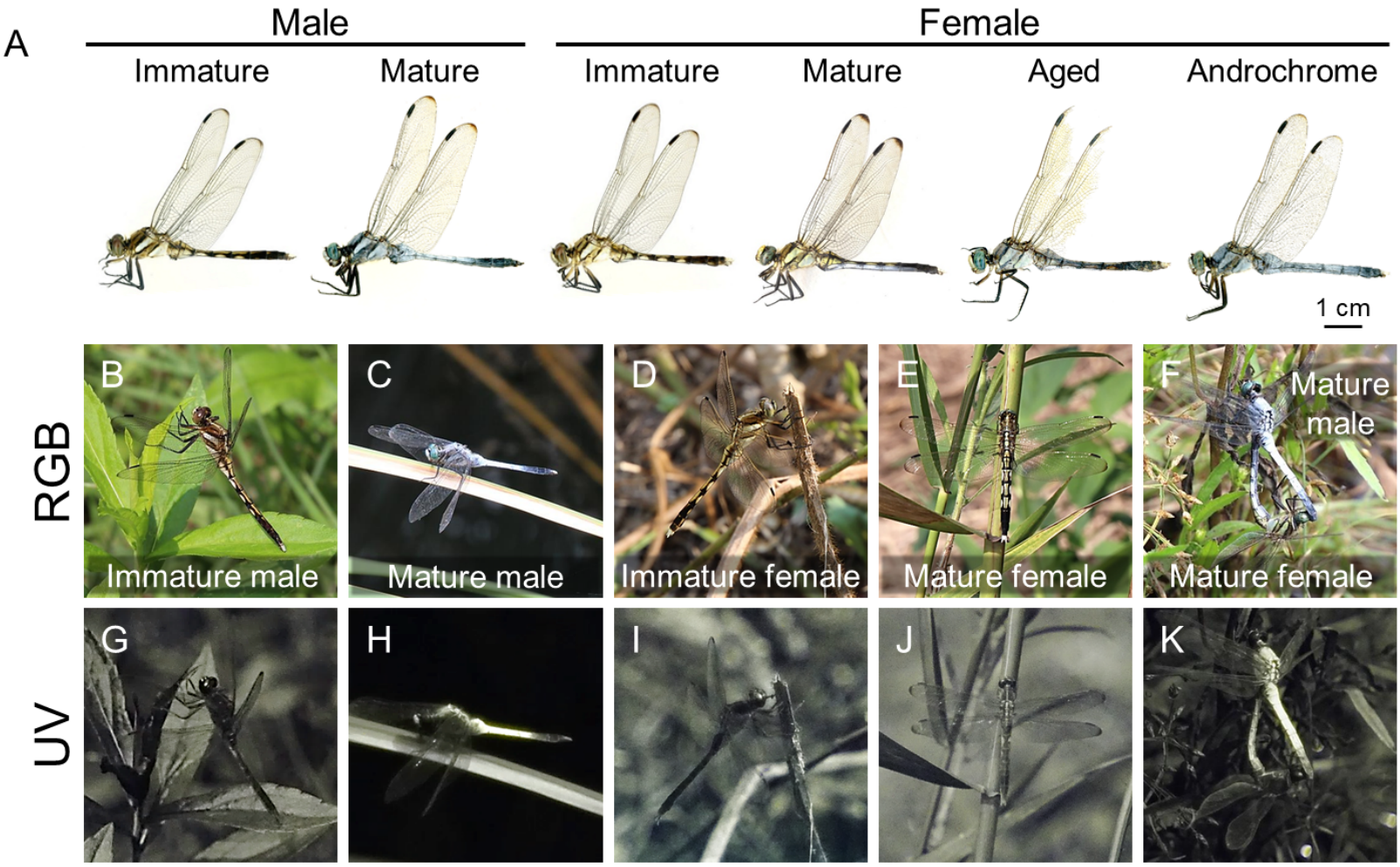
A
Male
Female
Immature
Mature
Immature
Mature
Aged
Androchrome
1 cm
RGB
UV
B
Immature male
C
Mature male
D
Immature female
E
Mature female
F
Mature male
Mature female
G
H
I
J
K

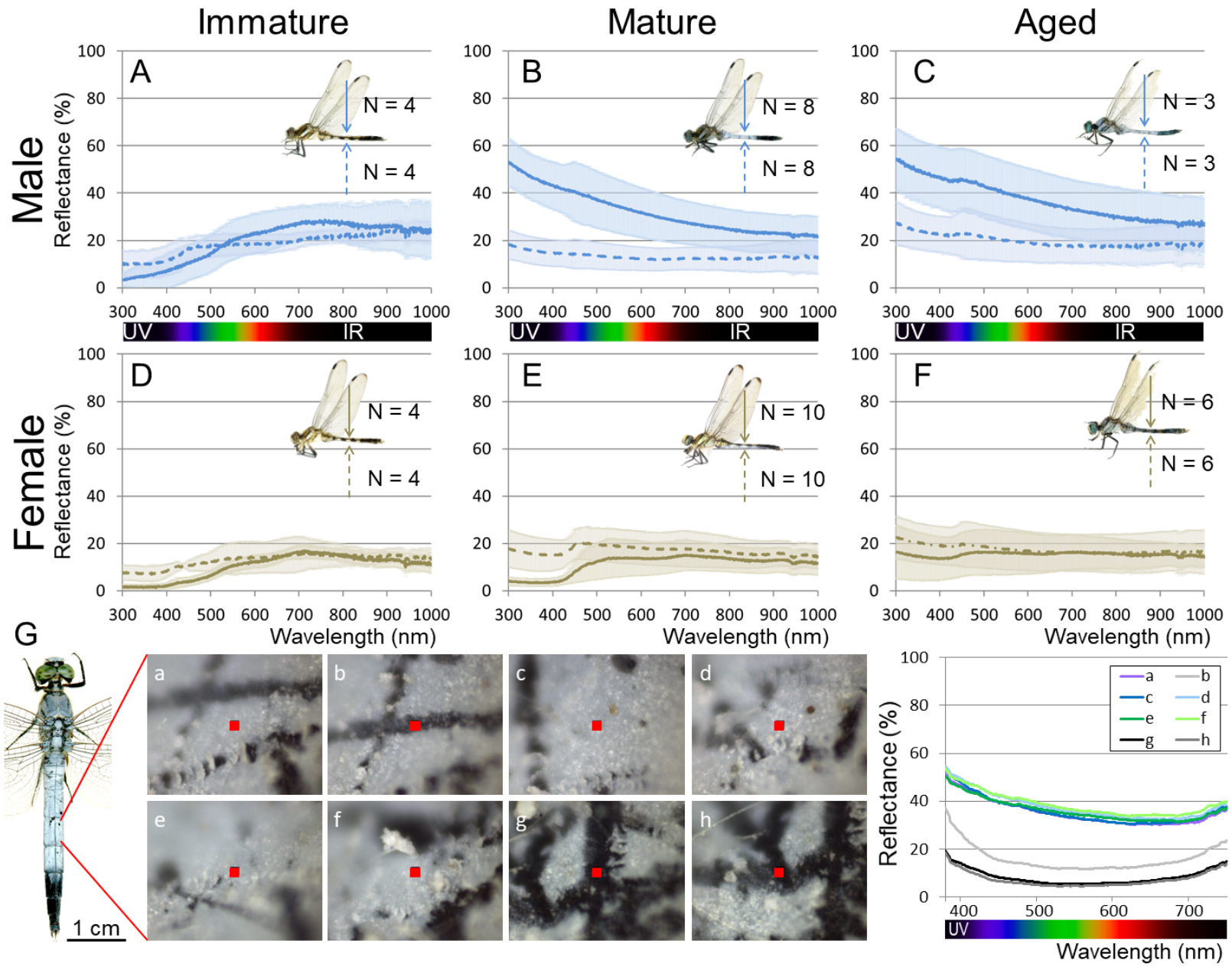
Immature
Mature
Aged
Male
Female
Reflectance (%)
A
B
C
D
E
F
N = 4
N = 4
N = 8
N = 8
N = 3
N = 3
N = 4
N = 4
N = 10
N = 10
N = 6
N = 6
UV
IR
Wavelength (nm)
G
a
b
c
d
e
f
g
h
1 cm
Reflectance (%)
Wavelength (nm)

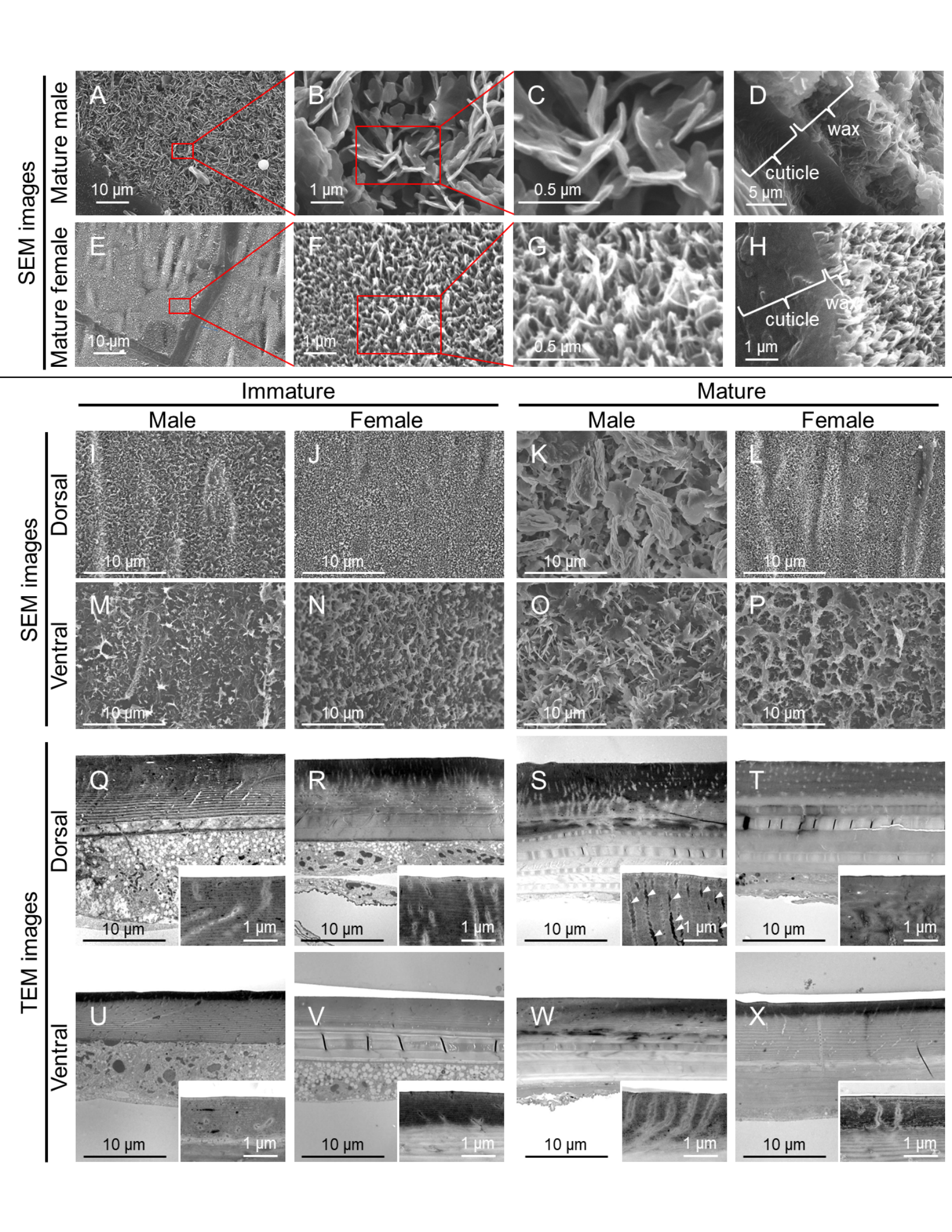
SEM images
Mature male
Mature female
A
B
C
D
wax
cuticle
10 μm
1 μm
0.5 μm
5 μm
E
F
G
H
wax
cuticle
10 μm
1 μm
0.5 μm
1 μm
Immature
Mature
Male
Female
Male
Female
SEM images
Dorsal
Ventral
I
J
K
L
M
N
O
P
10 μm
TEM images
Dorsal
Ventral
Q
R
S
T
U
V
W
X
10 μm
1 μm

A (Mature male, dorsal)

160 ± 1 °

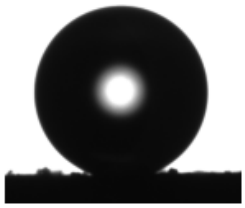

B (Mature male, dorsal + ethanol)

156 ± 4 °

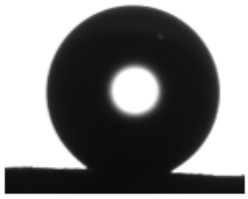

C (Mature male, dorsal + hexane)

121 ± 8 °

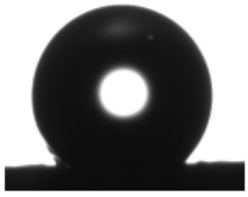

D (Mature male, dorsal + chloroform)

99 ± 4 °

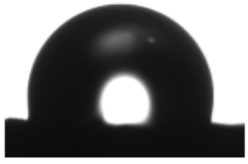

E

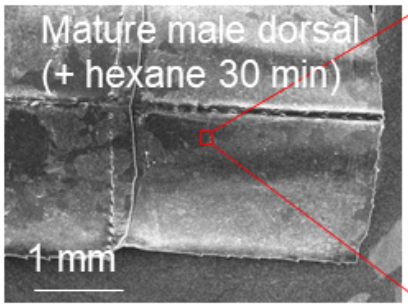

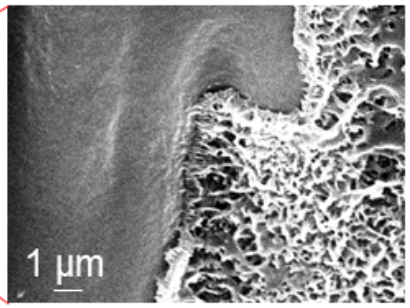

F

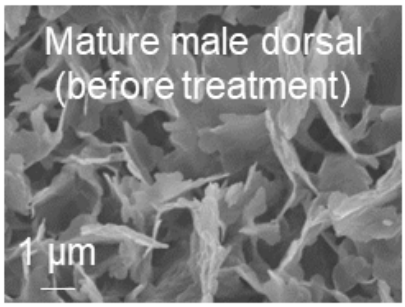

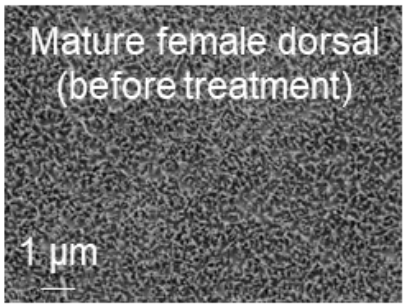

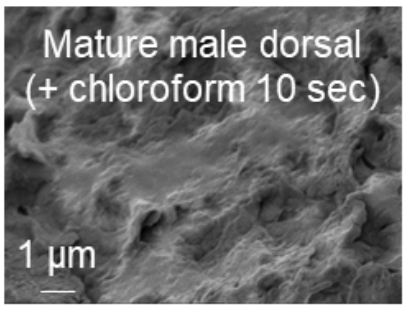

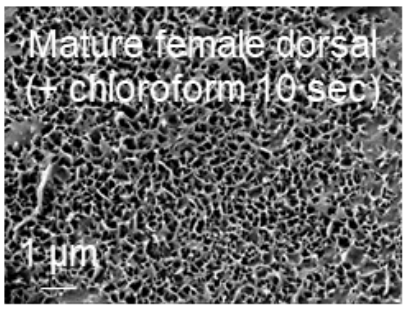

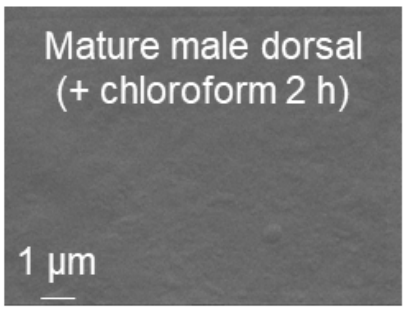

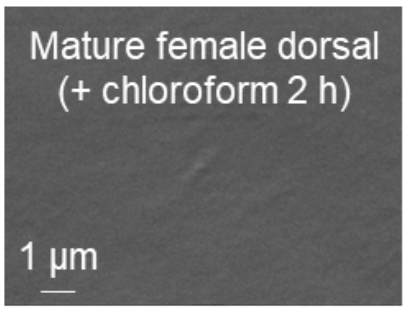

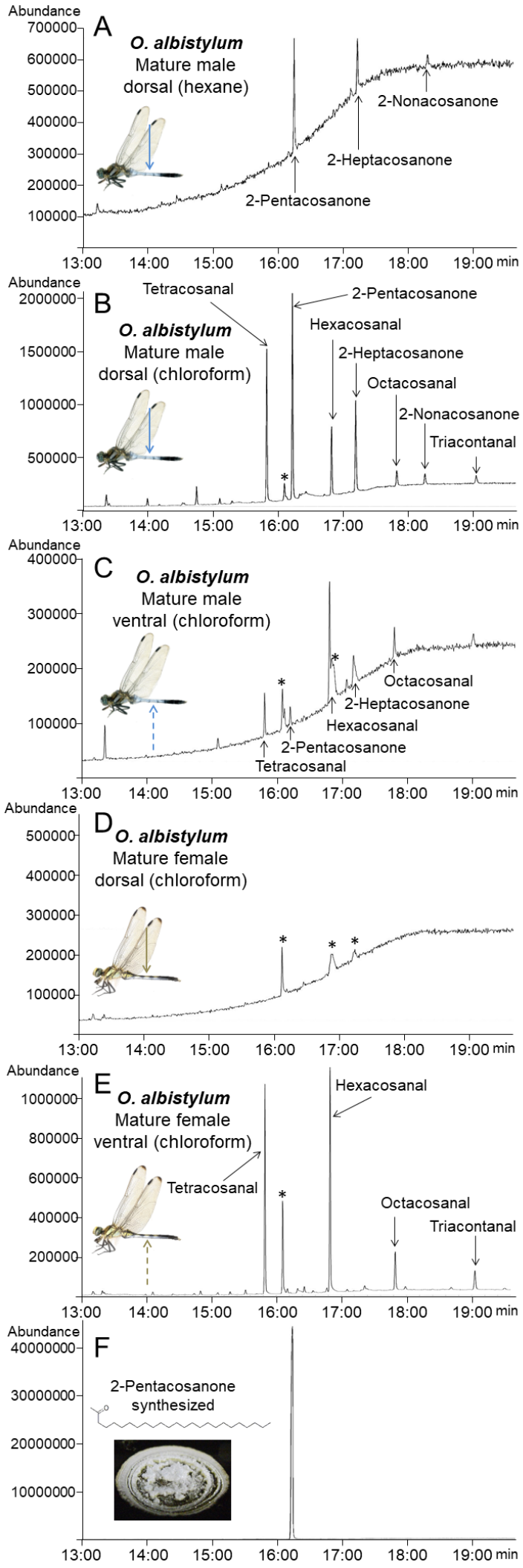
A
O. albistylum
Mature male
dorsal (hexane)
2-Nonacosanone
2-Heptacosanone
2-Pentacosanone
B
O. albistylum
Mature male
dorsal (chloroform)
Tetracosanal
2-Pentacosanone
Hexacosanal
2-Heptacosanone
Octacosanal
2-Nonacosanone
Triacontanal
C
O. albistylum
Mature male
ventral (chloroform)
Octacosanal
2-Heptacosanone
Hexacosanal
2-Pentacosanone
Tetracosanal
D
O. albistylum
Mature female
dorsal (chloroform)
E
O. albistylum
Mature female
ventral (chloroform)
Hexacosanal
Tetracosanal
Octacosanal
Triacontanal
F
2-Pentacosanone
synthesized
Abundance
13:00
14:00
15:00
16:00
17:00
18:00
19:00
min

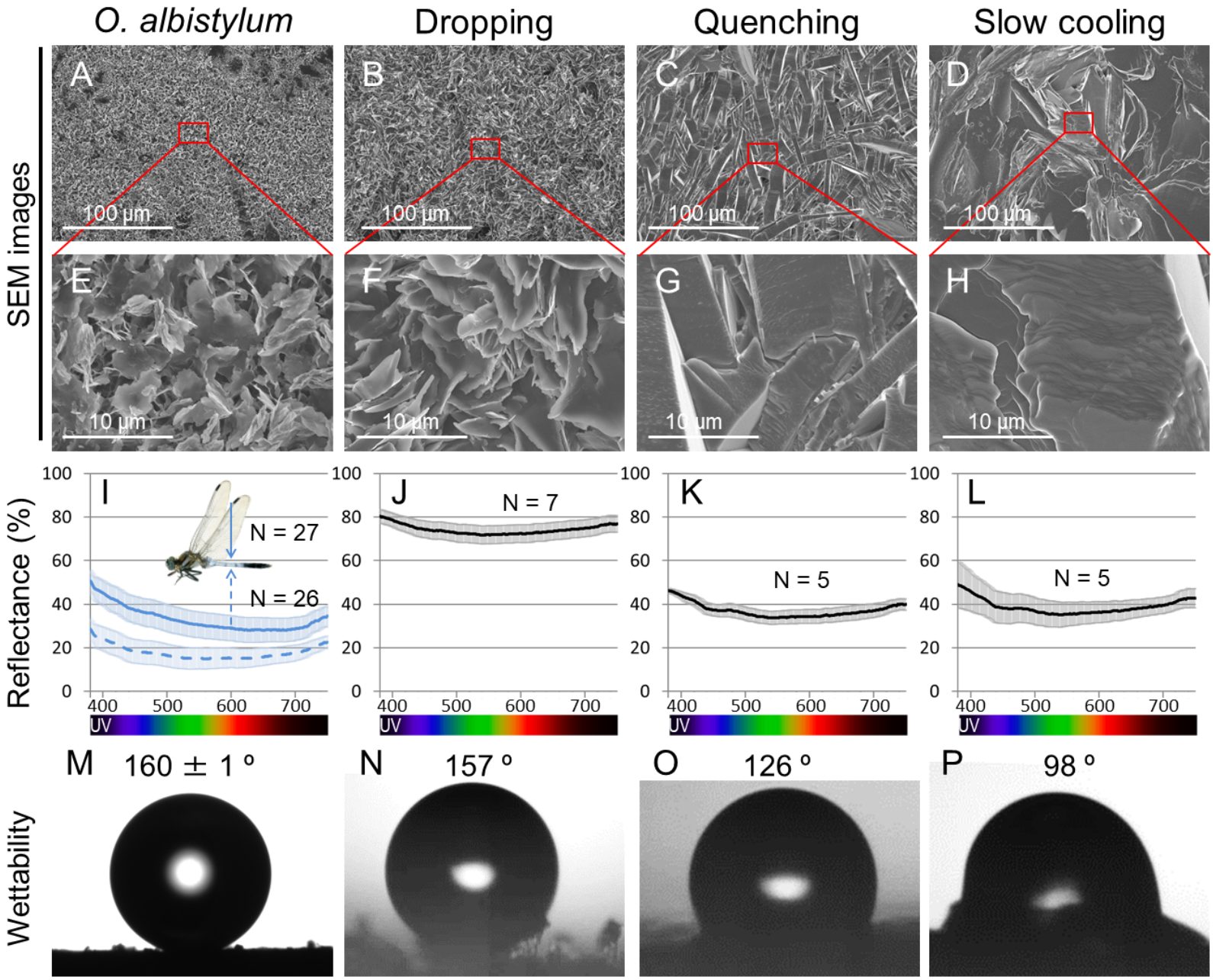
O. albistylum
Dropping
Quenching
Slow cooling
SEM images
A
B
C
D
E
F
G
H
100 µm
10 µm
Reflectance (%)
I
J
K
L
N = 27
N = 26
N = 7
N = 5
N = 5
UV
Wettability
M 160 ± 1 °
N 157 °
O 126 °
P 98 °

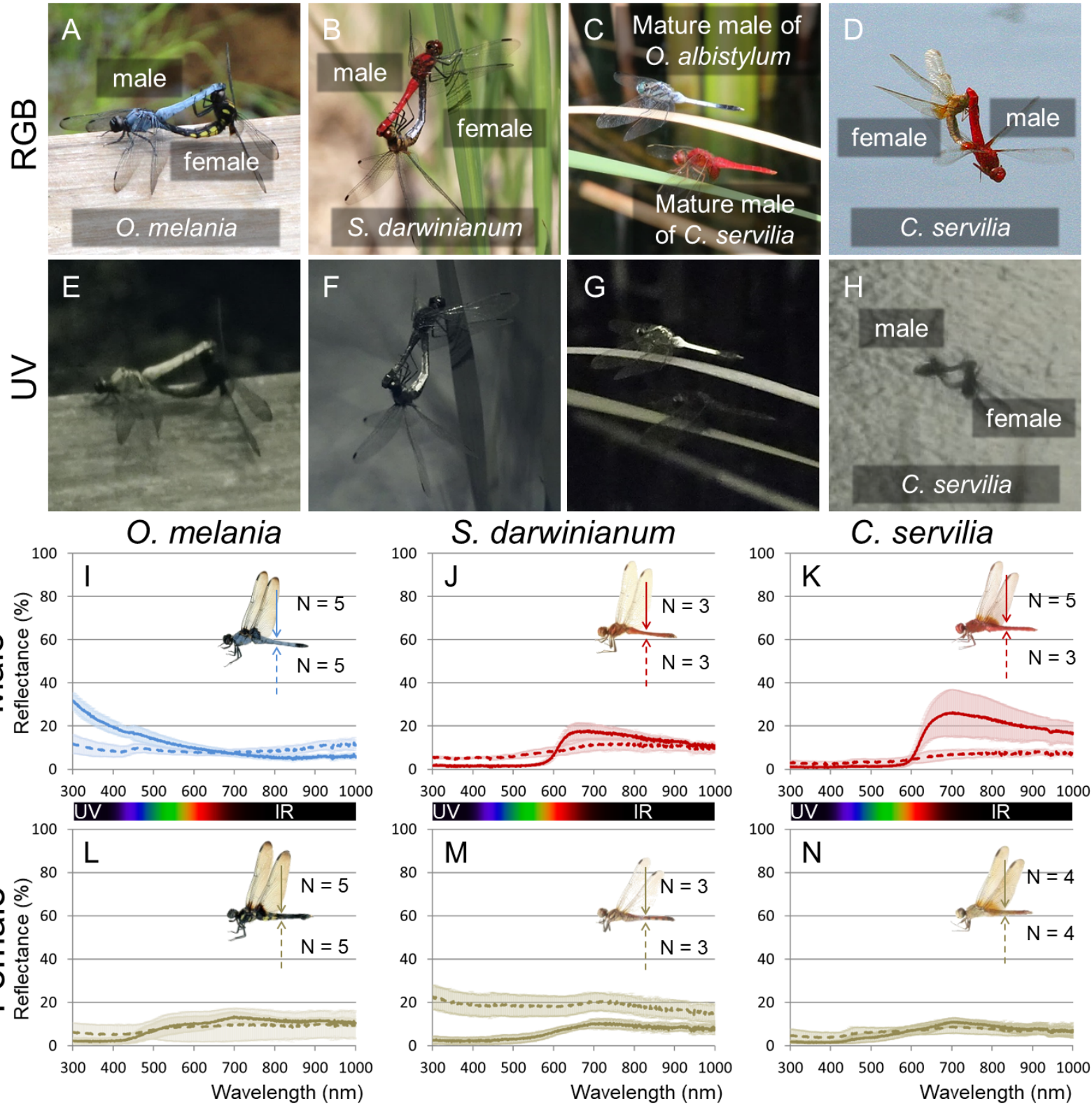
RGB
UV
A
male
female
O. melania
B
male
female
S. darwinianum
C
Mature male of O. albistylum
Mature male of C. servilia
D
female
male
C. servilia
E
F
G
H
male
female
C. servilia
O. melania
S. darwinianum
C. servilia
Male
Female
Reflectance (%)
I
J
K
L
M
N
N = 5
N = 3
N = 4
UV
IR
Wavelength (nm)

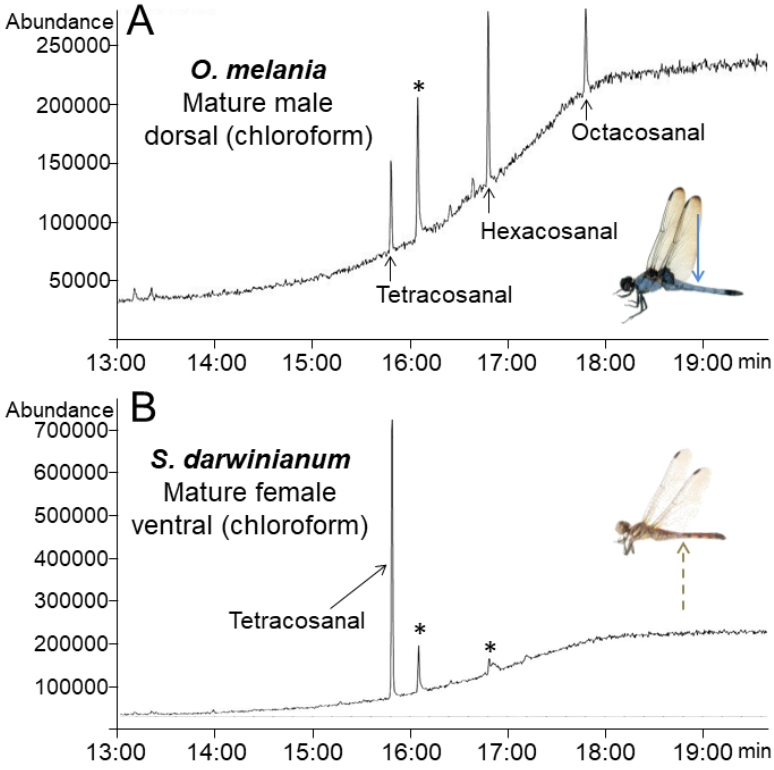

C

	Retention Time	15.8	16.2	16.8	17.2	17.8	18.2	19.0
	Molecular weight	334 352	366	362 380	394	390 408	422	418 436
	Candidate	Tetracosanal	2-Pentacosanone	Hexacosanal	2-Heptacosanone	Octacosanal	2-Nonacosanone	Triacontanal
Dorsal	*O. albistylum* male	+++	+++	++	+++	+	+	+
Dorsal	*O. albistylum* female							
Dorsal	*O. melania* male	++		++		++		
Dorsal	*O. melania* female							
Dorsal	*S. darwinianum* male							
Dorsal	*S. darwinianum* female							
Ventral	*O. albistylum* male	+	+	++	+	+		
Ventral	*O. albistylum* female	+++		+++		+		+
Ventral	*O. melania* male					+		
Ventral	*O. melania* female							
Ventral	*S. darwinianum* male							
Ventral	*S. darwinianum* female	+++						

A Mature male of *O. albistylum*

B Mature male of *O. melania*

C Mature male of *O. luzonicum*

D Mature male of *O. glaucum*

E Gynandromorph of *O. japonicum*

1 cm

F Gynandromorph of *L. pachygastra*

1 cm

A

B

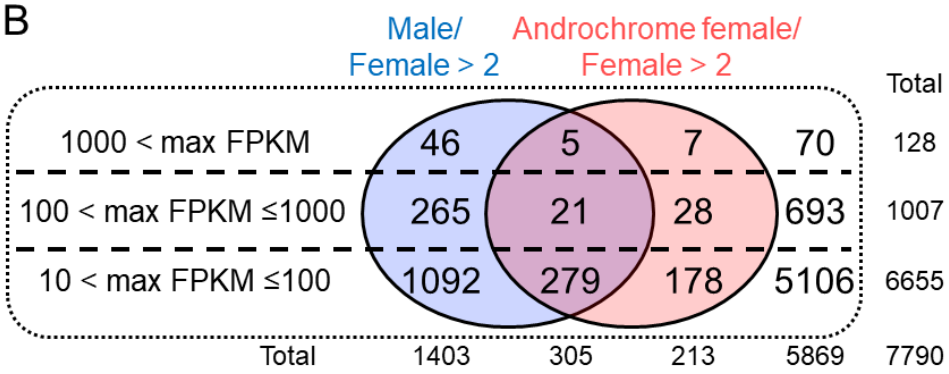

C

Description	Male										Female												Male /Female	Andro /Gyno
	Immature		Semimature		Mature		Mature-aged		Aged		Immature		Semimature		Mature		Mature-aged		Aged		Androchrome			
	D	V	D	V	D	V	D	V	D	V	D	V	D	V	D	V	D	V	D	V	D	V		
ELOVL fatty acid elongase 17 (LC416763)	159	17	5270	133	1613	50	766	9	664	67	7	2	6	5	5	4	6	21	163	21	844	132	334.6	144.7
Acyl-CoA Delta(11) desaturase (LC416764)	2	7	427	335	295	157	204	56	1553	1111	7	98	9	25	8	8	5	7	12	27	20	7	31.6	2.7
ferritin (LC416765)	81	470	403	814	441	511	1761	9208	2276	2571	28	205	168	379	82	189	113	289	1130	990	305	263	6.9	3.1
NPC intracellular cholesterol transporter 2 (LC416766)	217	47	1744	496	840	316	745	28	542	365	57	19	282	300	203	52	192	118	261	197	381	267	4.8	2.1
uncharacterized protein (LC416767)	131	638	1253	1457	4445	4726	4283	915	9927	8704	248	2535	1051	1596	851	1111	593	770	797	1064	2535	1684	3.7	3.7

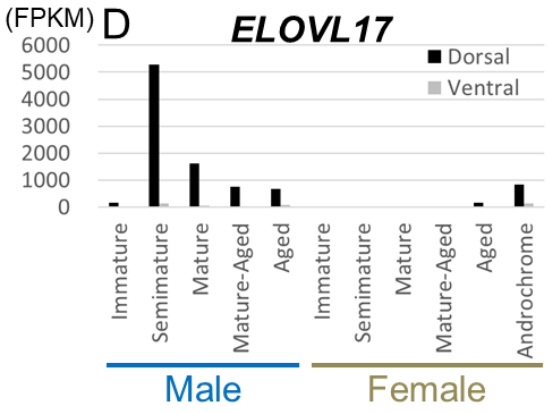

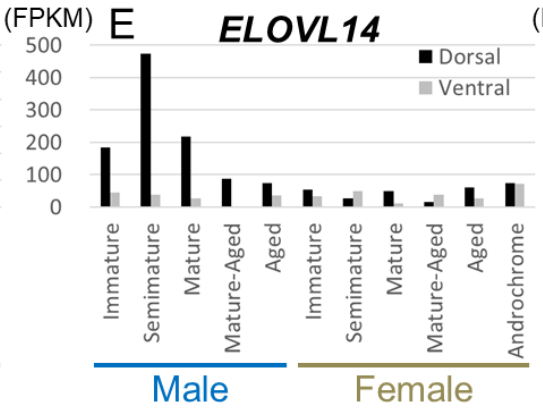

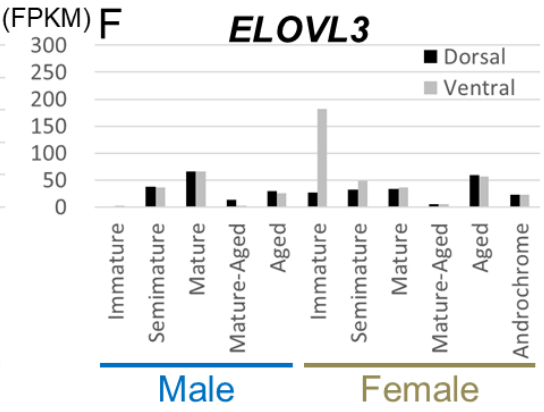

A

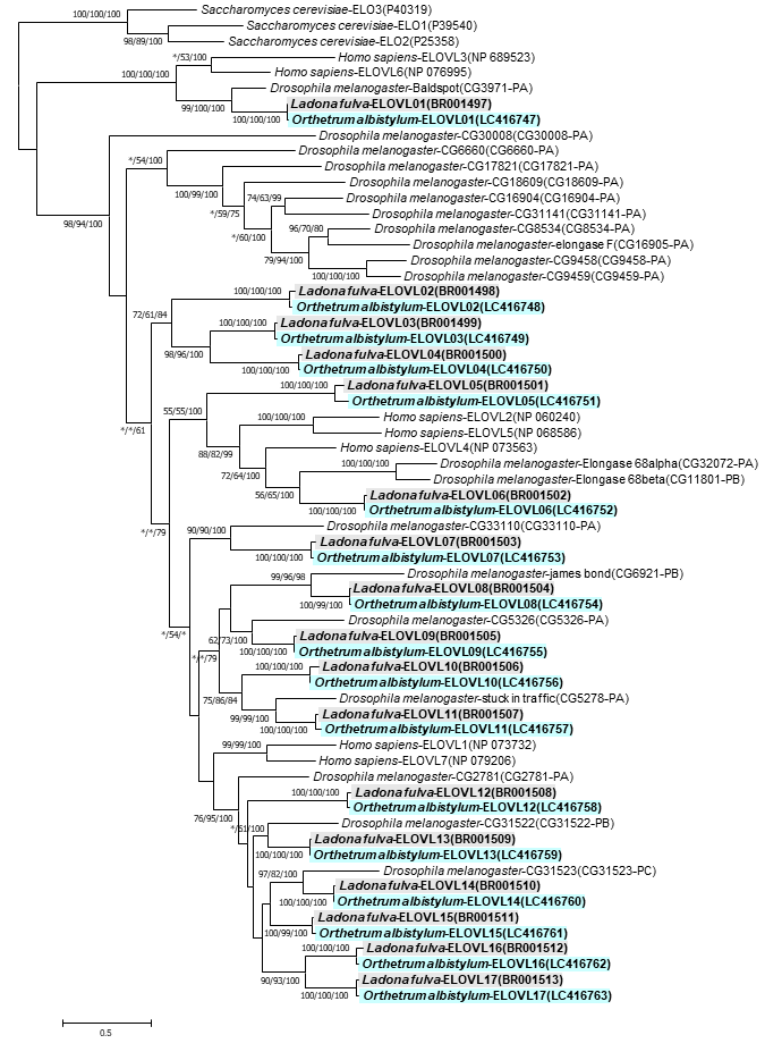

B

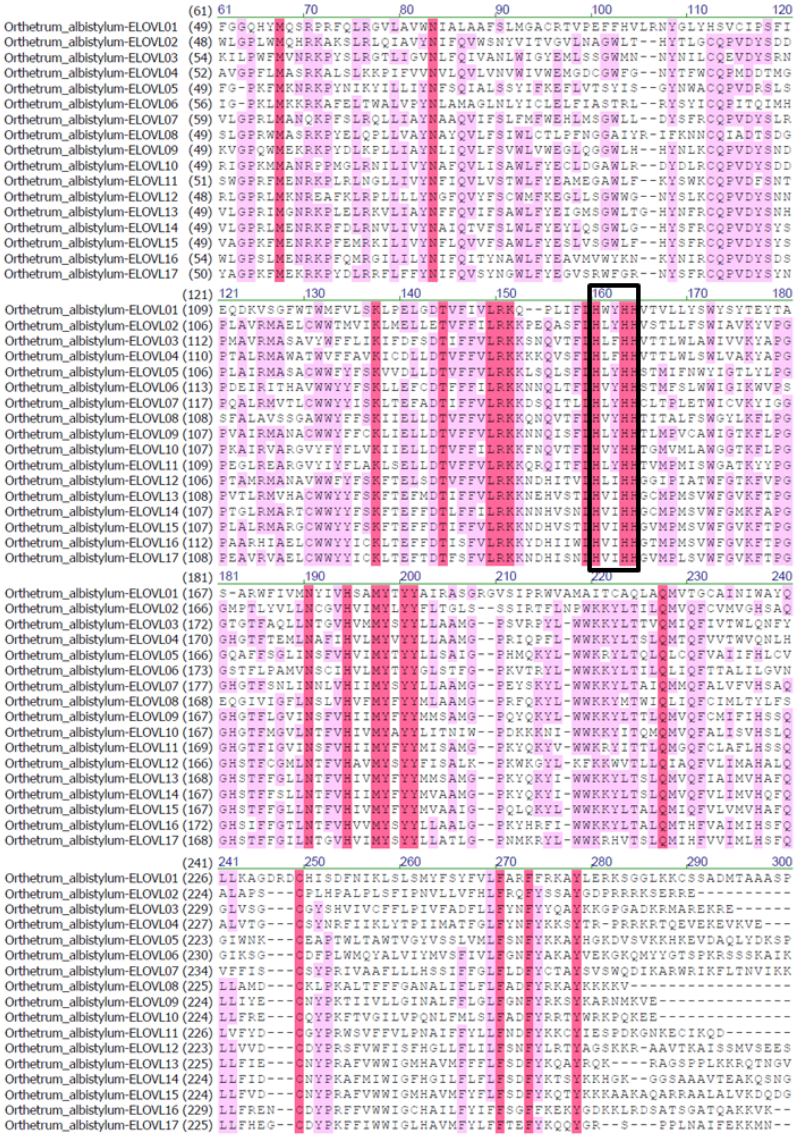

C

	Male										Female													
	Immature		Semimature		Mature		Mature-aged		Aged		Immature		Semimature		Mature		Mature-aged		Aged		Androchrome		Male /Female	Andro /Gyno
	D	V	D	V	D	V	D	V	D	V	D	V	D	V	D	V	D	V	D	V	D	V		
ELOVL fatty acid elongase 1 (LC416747)	57	11	74	23	18	10	19	7	14	10	24	9	27	14	14	3	13	8	19	11	18	18	2.1	0.9
ELOVL fatty acid elongase 2 (LC416748)	0	0	0	0	0	0	0	0	0	0	0	0	0	0	0	0	0	0	0	0	0	0	0.0	0.0
ELOVL fatty acid elongase 3 (LC416749)	0	3	38	36	66	67	14	3	30	25	27	182	32	49	33	37	5	5	60	56	23	23	1.2	0.9
ELOVL fatty acid elongase 4 (LC416750)	0	0	0	0	0	0	0	0	0	0	0	0	0	0	0	0	0	0	0	0	0	0	0.0	0.0
ELOVL fatty acid elongase 5 (LC416751)	2	0	0	0	0	0	0	0	0	0	1	2	0	1	0	0	0	0	0	0	0	0	1.7	0.2
ELOVL fatty acid elongase 6 (LC416752)	2	5	0	0	0	0	0	0	0	3	0	0	0	0	26	24	1	11	1	0	7	198	0.1	1.1
ELOVL fatty acid elongase 7 (LC416753)	2	10	0	1	0	0	0	0	0	1	0	0	0	0	0	0	0	0	0	0	0	0	6.7	0.0
ELOVL fatty acid elongase 8 (LC416754)	0	1	0	0	0	0	0	0	1	1	0	0	0	0	5	5	0	5	0	0	1	26	0.2	0.9
ELOVL fatty acid elongase 9 (LC416755)	672	111	49	17	41	16	102	6	27	28	57	15	37	14	44	16	45	33	76	30	65	17	4.7	1.4
ELOVL fatty acid elongase 10 (LC416756)	0	1	0	0	0	0	0	0	0	0	0	0	2	0	0	0	0	0	0	0	0	1	0.0	0.0
ELOVL fatty acid elongase 11 (LC416757)	28	5	6	0	5	1	10	0	2	2	23	3	4	2	0	0	2	1	1	1	0	0	1.7	0.0
ELOVL fatty acid elongase 12 (LC416758)	4	1	0	0	0	0	0	0	0	0	0	0	0	0	0	0	0	0	0	0	0	0	47.7	0.0
ELOVL fatty acid elongase 13 (LC416759)	4	28	51	7	23	6	11	5	10	7	5	3	1	1	9	5	2	7	2	3	38	16	5.0	8.5
ELOVL fatty acid elongase 14 (LC416760)	185	44	473	37	217	26	87	3	73	36	54	33	27	49	49	11	16	38	60	27	73	73	6.6	2.0
ELOVL fatty acid elongase 15 (LC416761)	98	42	14	8	11	7	8	1	1	4	80	29	7	7	39	10	25	25	7	5	2	21	0.9	0.1
ELOVL fatty acid elongase 16 (LC416762)	2	1	1	1	0	0	0	0	0	0	1	1	4	2	0	0	0	0	0	0	0	0	0.6	0.0
ELOVL fatty acid elongase 17 (LC416763)	159	17	5270	133	1613	50	766	9	664	67	7	2	6	5	5	4	6	21	163	21	844	132	334.6	144.7

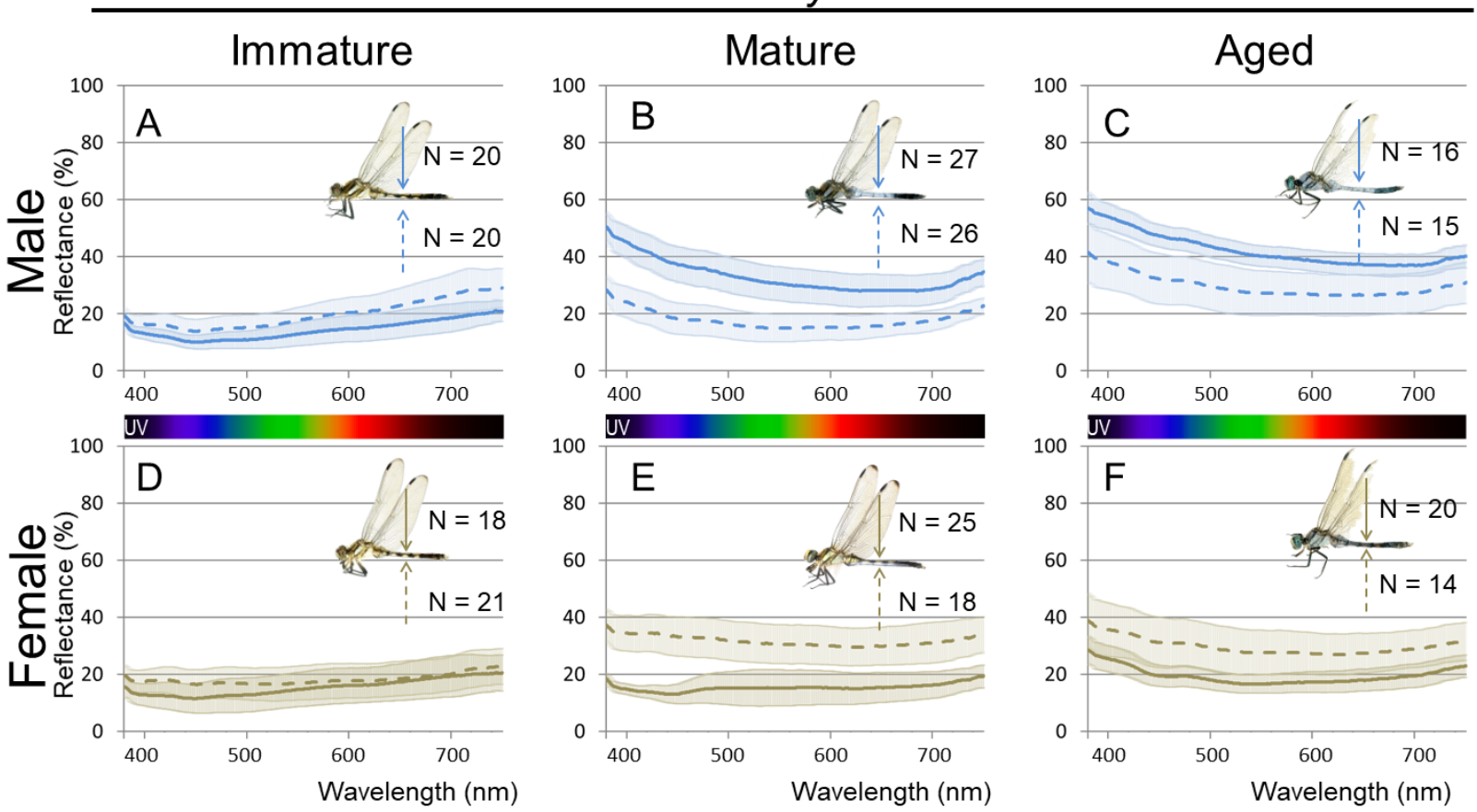
O. albistylum
Immature
Mature
Aged
Male
Female
Reflectance (%)
A
B
C
D
E
F
N = 20
N = 20
N = 27
N = 26
N = 16
N = 15
N = 18
N = 21
N = 25
N = 18
N = 20
N = 14
UV
Wavelength (nm)

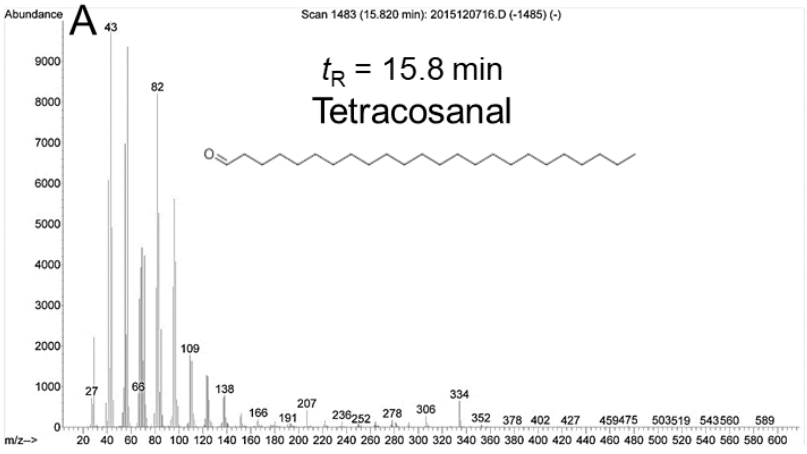
A
Scan 1483 (15.820 min): 2015120716.D (-1485) (-)
t_R = 15.8 min
Tetracosanal

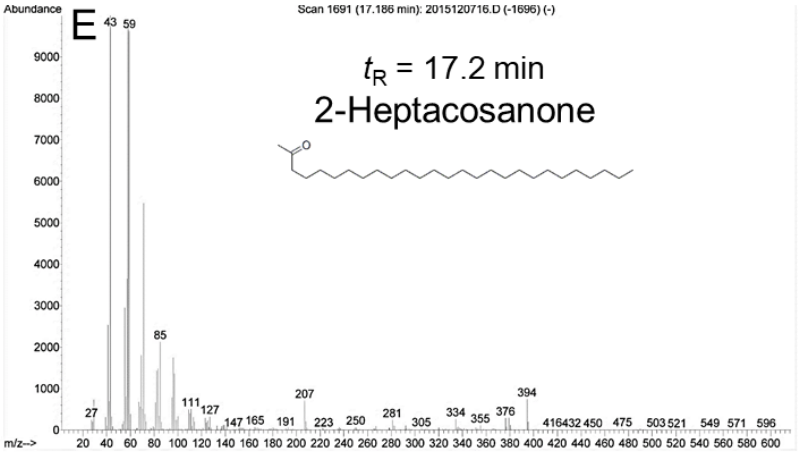
E
Scan 1691 (17.186 min): 2015120716.D (-1695) (-)
t_R = 17.2 min
2-Heptacosanone

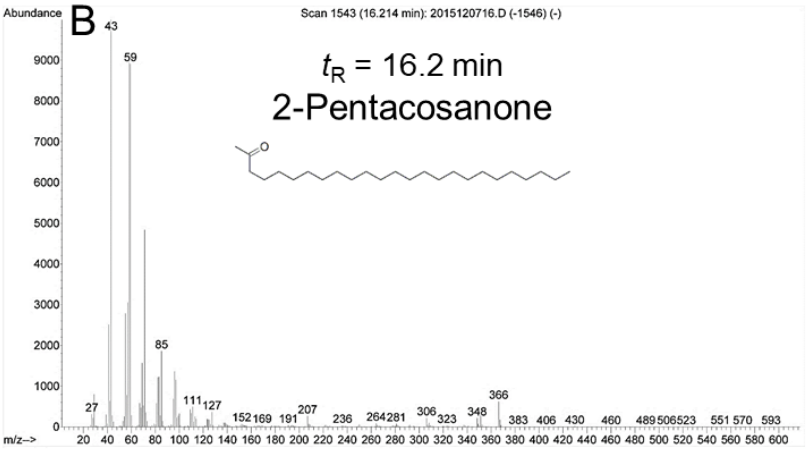
B
Scan 1543 (16.214 min): 2015120716.D (-1546) (-)
t_R = 16.2 min
2-Pentacosanone

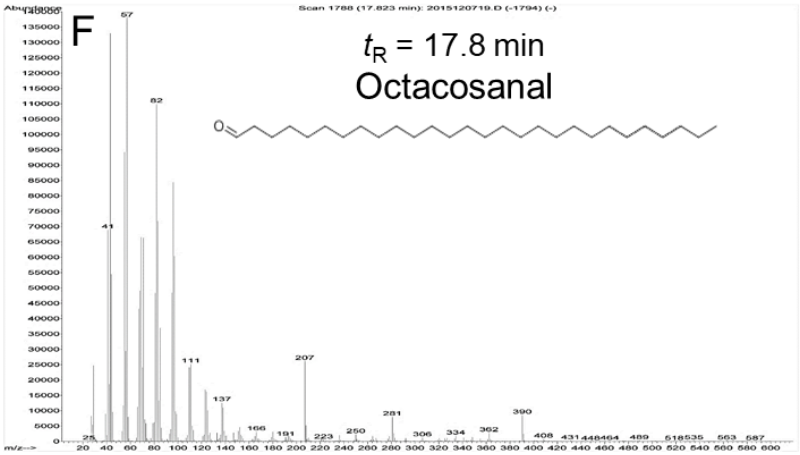
F
t_R = 17.8 min
Octacosanal

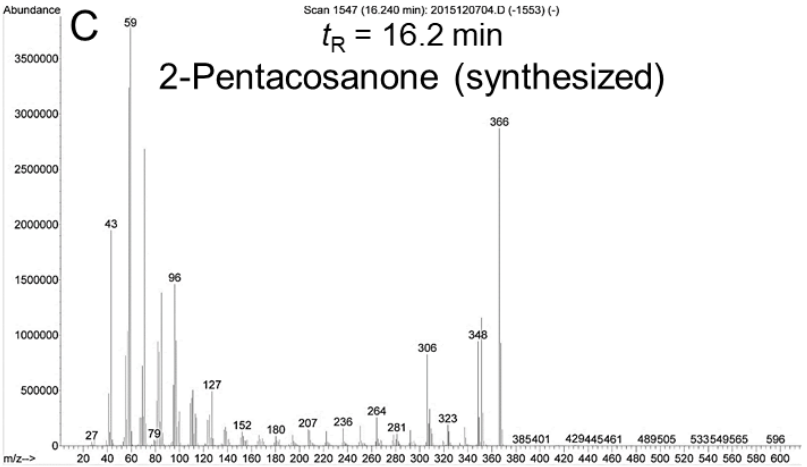
C
Scan 1547 (16.240 min): 2015120704.D (-1553) (-)
t_R = 16.2 min
2-Pentacosanone (synthesized)

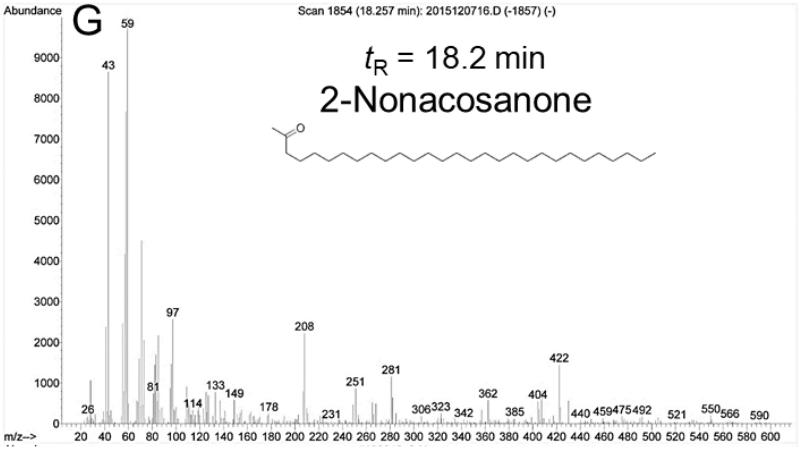
G
Scan 1854 (18.257 min): 2015120716.D (-1857) (-)
t_R = 18.2 min
2-Nonacosanone

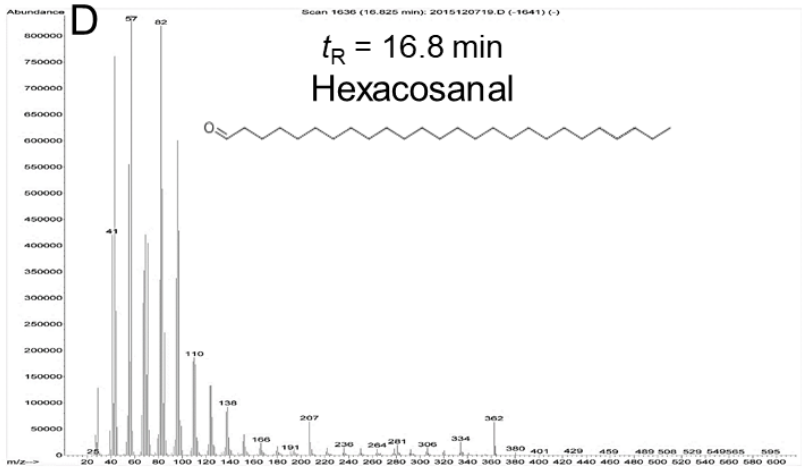
D
t_R = 16.8 min
Hexacosanal

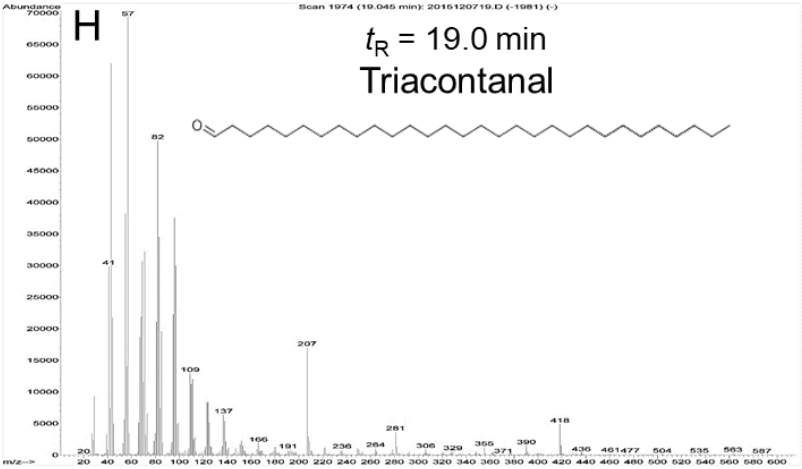
H
t_R = 19.0 min
Triacontanal

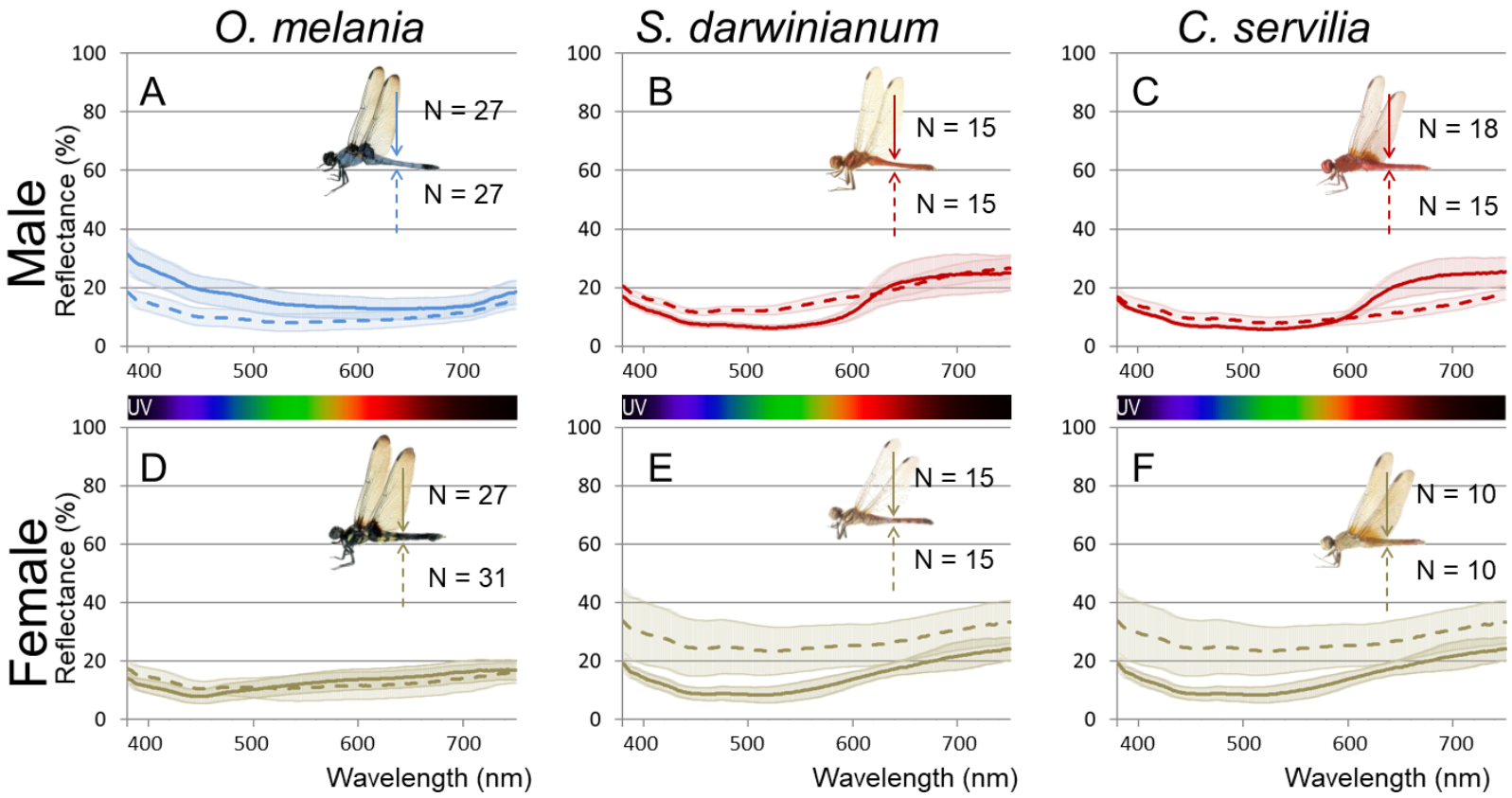
O. melania
S. darwinianum
C. servilia
Male
Female
Reflectance (%)
A
B
C
D
E
F
N = 27
N = 27
N = 15
N = 15
N = 18
N = 15
N = 27
N = 31
N = 15
N = 15
N = 10
N = 10
UV
Wavelength (nm)

	Immature		Semimature		Mature		Mature-aged		Aged		Immature		Semimature		Mature		Mature-aged		Aged		Androchrome					
contig	D	V	D	V	D	V	D	V	D	V	D	V	D	V	D	V	D	V	D	V	D	V	Description (Top hit)	E-value	Male /Female	Andro /Gyno	Max FPKM (Dorsal)
c153509R	131	638	1253	1457	4445	4726	4283	915	9927	8704	248	2535	1051	1596	851	1111	588	770	797	1064	2535	1684	NA		3.7	3.7	9927
c147539R (ELOVL17)	159	17	5270	133	1613	50	766	9	664	67	7	2	6	5	5	4	6	21	163	21	844	132	elongation of very long chain fatty acids protein AAEL008004 [Camponotus floridanus]	3.00E-122	334.6	144.7	5270
c148747R	81	470	403	814	441	511	1761	9208	2276	2571	28	205	168	379	82	189	113	289	1130	990	305	263	ferritin [Ornithodoros parkeri]	1.00E-69	6.9	3.1	2276
c153703R	217	47	1744	496	840	316	745	28	542	365	57	19	282	300	203	52	192	118	261	197	381	267	NPC intracellular cholesterol transporter 2 [Agrilus planipennis]	2.00E-44	4.8	2.1	1744
c145398R	2	7	427	335	295	157	204	56	1553	1111	7	98	9	25	8	8	5	7	12	27	20	7	Acyl-CoA Delta(11) desaturase [Zootermopsis nevadensis]	0	31.6	2.7	1553
c143830R	15	8	110	12	689	19	89	6	47	93	15	12	12	6	9	7	8	18	57	18	56	38	Serine protease inhibitor I/II [Lygus hesperus]	4.00E-24	20.9	5.1	689
c142423R (ELOVL14)	185	44	473	37	217	26	87	3	73	36	54	33	27	49	49	11	16	38	60	27	73	73	elongation of very long chain fatty acids protein AAEL008004 [Camponotus floridanus]	2.00E-158	6.6	2.0	473
c145528R	52	52	445	79	238	54	149	15	258	166	36	65	63	71	76	21	26	47	78	88	200	126	mid1-interacting protein 1-like [Zootermopsis nevadensis]	3.00E-70	4.4	4.0	445
c139626R	1	0	91	144	33	54	97	47	54	211	1	1	11	1	45	27	15	4	370	222	37	59	CG9269 [Drosophila melanogaster]	5.00E-16	3.1	2.1	370
c149278R	18	9	284	139	174	64	58	4	111	70	12	16	33	20	52	10	9	11	31	15	53	21	acetyl-coenzyme A synthetase [Zootermopsis nevadensis]	0	5.0	2.0	284
c146555R	3	0	29	48	130	142	275	48	0	0	0	0	18	55	32	44	34	47	0	0	49	31	CG34166 [Drosophila melanogaster]	1.00E-13	5.3	2.4	275
c153289R	262	805	93	133	143	187	167	29	79	99	28	92	84	124	97	78	57	71	256	278	227	89	apolipoprotein D-like [Zootermopsis nevadensis]	4.00E-65	2.5	3.4	262
c151984R	1	3	32	33	114	51	31	4	248	179	1	2	6	5	11	14	5	5	8	9	41	14	trehalose-6-phosphate synthase 1 [Blattella germanica]	0	8.0	7.3	248
c149439R	0	0	205	20	0	0	24	1	4	17	11	1	1	0	0	7	5	20	0	0	22	42	tyrosine 3-monooxygenase [Zootermopsis nevadensis]	0	13.2	5.0	205
c149196R	33	27	48	51	109	114	142	107	108	90	27	51	1	0	23	15	72	101	60	51	197	213	40S ribosomal protein S15 [Blattella germanica]	2.00E-64	2.7	6.4	197
c150668R	3	14	55	76	51	37	192	43	142	97	5	38	21	34	14	14	8	10	27	37	25	11	mitochondrial basic amino acids transporter [Cryptotermes secundus]	8.00E-104	6.1	2.1	192
c146712R	71	30	157	166	20	15	70	55	14	0	2	1	8	6	12	3	3	8	31	33	14	49	cystathionine gamma-lyase [Crassostrea gigas]	0	13.1	2.3	157
c148028R	23	4	155	8	40	5	20	1	14	4	6	4	9	7	3	2	2	5	5	2	18	13	putative fatty acyl-CoA reductase [Cryptotermes secundus]	0	12.3	3.7	155
c154118R	10	8	48	98	141	122	55	16	108	88	3	8	4	0	49	62	16	29	38	52	61	39	icarapin-like [Orussus abietinus]	2.00E-18	3.5	3.3	141
c153348R	41	87	130	63	34	45	23	32	88	73	21	19	42	35	30	22	20	26	48	40	60	19	ATP-binding cassette sub-family G member 4 [Cryptotermes secundus]	0	2.0	2.1	130
c149130R	40	11	125	39	37	31	20	3	28	13	13	5	9	7	25	2	10	13	46	17	32	41	Serine protease inhibitor 88Ea [Blattella germanica]	5.00E-95	3.9	2.2	125
c150904R	60	262	63	68	120	125	101	25	80	78	16	75	61	96	46	51	40	48	93	96	91	29	hypothetical protein B7P43_G14218 [Cryptotermes secundus]	3.00E-58	2.1	2.2	120
c147603R	38	137	71	85	119	135	68	32	38	35	2	41	3	4	0	0	39	63	11	21	34	20	Regenectin [Periplaneta americana]	4.00E-51	6.7	3.1	119
c153222R	0	0	92	69	13	32	119	63	11	17	0	4	14	28	2	8	2	11	13	29	39	14	kynurenine/alpha-aminoadipate aminotransferase [Habropoda laboriosa]	2.00E-130	12.4	8.7	119
c148957R	1	6	49	56	72	48	95	19	118	88	0	7	4	3	23	32	13	17	21	19	29	13	NA		5.4	2.9	118
c148343R	1	6	27	36	54	45	41	10	117	62	1	7	5	3	2	2	4	2	36	52	28	14	chitotriosidase-1 [Megachile rotundata]	8.00E-26	10.1	9.2	117
c149270R	9	5	64	29	102	88	35	16	40	32	23	18	40	30	29	13	8	20	7	2	54	45	pyruvate kinase-like [Cryptotermes secundus]	0	2.1	2.2	102